Macrophage-derived glutamine boosts satellite cells and muscle regeneration

Min Shang[1,2], Federica Cappellesso[1,2], Ricardo Amorim[1,2,3,4], Jens Serneels[1,2], Federico Virga[1,2,5,6], Guy Eelen[7,8], Stefania Carobbio[9], Melvin Y. Rincon[10,11,12], Pierre Maechler[9], Katrien De Bock[13], Ping-Chih Ho[14], Marco Sandri[15,16,17], Bart Ghesquière[18,19], Peter Carmeliet[7,8], Mario Di Matteo[1,2], Emanuele Berardi[1,2,#,§], and Massimiliano Mazzone[1,2,20,#, §]

1. Laboratory of Tumor Inflammation and Angiogenesis, Center for Cancer Biology, VIB, Leuven, B3000, Belgium; **2.** Laboratory of Tumor Inflammation and Angiogenesis, Center for Cancer Biology, Department of Oncology, KU Leuven, Leuven, B3000, Belgium; **3.** Life and Health Sciences Research Institute, School of Medicine, University of Minho, Campus de Gualtar, Braga, 4710-057, Portugal; **4.** ICVS/3B's-PT Government Associate Laboratory, Braga/Guimarães, 4710-057, Portugal; **5.** Molecular Biotechnology Center, University of Torino, Torino, Italy; **6.** Department of Molecular Biotechnology and Health Sciences, University of Torino, Torino, Italy; **7.** Laboratory of Angiogenesis and Vascular Metabolism, Center for Cancer Biology, VIB, Leuven, B3000, Belgium; **8.** Laboratory of Angiogenesis and Vascular Metabolism, Center for Cancer Biology, Department of Oncology, KU Leuven, Leuven, B3000, Belgium; **9.** Department of Cell Physiology and Metabolism, University of Geneva Medical Center, 1211 Geneva, Switzerland; **10.** VIB-KU Leuven Center for Brain & Disease Research, Leuven, B3000, Belgium; **11.** KU Leuven, Department of Neuroscience, Leuven, B3000, Belgium; **12.** Centro de Investigaciones, Fundacion Cardiovascular de Colombia, Floridablanca, 681004, Colombia; **13.** Department of Health Sciences and Technology, ETH, Zurich, 8603, Switzerland; **14.** Department of Oncology, Ludwig Cancer Research, University of Lausanne, Biopole 3 - 02DB92, Chemin des Boveresses 155, CH-1066 Epalinges, Switzerland; **15.** Venetian Institute of Molecular Medicine, Padova, 35129, Italy; **16.** Department of Biomedical Science, University of Padova, Padova, 35100, Italy; **17.** Department of Medicine, McGill University, Montreal, QC H4A 3J1, Canada; **18.** Metabolomics Core Facility, Center for Cancer Biology, VIB, Leuven, B3000, Belgium; **19**. Metabolomics Core Facility, Center for Cancer Biology, Department of Oncology, KU Leuven, Leuven, B3000, Belgium; **20.** Department of Molecular Biotechnology and Health Science, Molecular Biotechnology Centre, University of Torino, Torino, Italy. **#** equal contributors.

[§]**Editorial correspondence to**: M. Mazzone: massimiliano.mazzone@kuleuven.vib.be

E. Berardi: emanuele.berardi@kuleuven.vib.be

Running title: A macrophage-satellite cell metabolic cross-talk

Muscle regeneration is sustained by infiltrating macrophages and consequent satellite cell (SC) activation[1-4]. Macrophages and SC communicate in different ways[1-5] but their metabolic interplay was never investigated so far. Here, we found that muscle injuries and aging are characterized by intratissutal glutamine restriction. Low glutamine levels endow macrophages with the metabolic ability to secrete glutamine via enhanced glutamine synthetase (GS) activity at the expense of glutamate dehydrogenase-1 (GLUD1)-mediated glutamine oxidation. *Glud1* knockout (KO) macrophages display constitutively high GS activity which prevents glutamine shortage. Import of macrophage-derived glutamine by SC through the glutamine-transporter SLC1A5 activates mTOR and promotes SC proliferation and differentiation. Consequently, macrophage-specific deletion or pharmacological inhibition of GLUD1 improves muscle regeneration and functional recovery in response to acute injury, ischemia, or aging. Conversely, SLC1A5 blockade in SC or GS inactivation in macrophages negatively affects SC functions and muscle regeneration. These results highlight a metabolic cross-talk between SC and macrophages whereby macrophage-derived glutamine sustains SC functions. Thus, GLUD1 targeting offers new therapeutic opportunities for the regeneration of injured or aged muscles.

Macrophages contribute to the repair of damaged skeletal muscle[3,5]. These cells clear tissue debris and release cytokines as well as growth factors that stimulate SC proliferation[4-6]. Later, macrophages promote SC differentiation[4-7], and tissue revascularization[7]. The positive involvement of inflammatory cells in the acute phase of muscle healing is supported by the evidence that macrophage depletion impairs muscle regenerative capacity[8].

Given the important role of glutamine in muscle homeostasis[9-11], and our observation that glutamine production by macrophages remodels the composition of the extracellular tumor

milieu[12,13], we hypothesized a function of glutamine in a yet unidentified, metabolic cross-talk between macrophages and SC.

To induce myofiber death, inflammation and muscle regeneration, we injected cardiotoxin (CTX) in the *tibialis anterior* (TA)[14] or provoked ischemia of the crural muscles[15] in control (CTRL) and Glud1$^{\Delta Mo}$ mice, with complete GLUD1 deletion in macrophages and only 38% knockdown in neutrophils (Extended Data Fig. 1a-c). CTRL and Glud1$^{\Delta Mo}$ mice revealed similar muscle histology in healthy conditions and early after damage, *i.e.* 1 day post-CTX or 3 days post-femoral-artery-ligation (Fig. 1a-e). However, compared to CTRL, Glud1$^{\Delta Mo}$ mice displayed an earlier peak in the number of regenerating myofibers and a quicker resolution of muscle necrosis, cell death, oxidative damage, and inflammation (Fig. 1a-m). Six days post-CTX, muscle viability was higher in Glud1$^{\Delta Mo}$ *vs.* CTRL mice. Yet, the early regenerating myofibers (expressing embryonic myosin heavy chain) were fewer, but the late ones (negative for embryonic myosin heavy chain) were larger in Glud1$^{\Delta Mo}$ mice, pointing to a faster and more advanced regeneration (Fig. 1n-p). This phenotype was due to monocyte-derived macrophages, rather than tissue-resident macrophages (Extended Data Fig. 1d,e). Inducible deletion of *Glud1* in macrophages only led to improved muscle recovery as well (Extended Data Fig. 1f-i).

In voluntary wheel running tests, the baseline physical activity and its drop 1 day post-CTX were comparable in both genotypes. However, Glud1$^{\Delta Mo}$ mice re-gained the pre-injured physical capabilities earlier than CTRL mice (Fig. 1q).

Basal numbers of SC, assessed by Pax7 expression[16], was comparable between genotypes (Fig. 1r-v). However, after injury, induction of SC proliferation (assessed by PHH3, or Ki67) and differentiation (assessed by the early and late differentiation markers MyoD and

Myogenin, respectively[17]) were stronger and quicker in Glud1$^{\Delta Mo}$ than in CTRL mice (Fig. 1r-x; Extended Data Fig. 1j-n). Thus, muscle regeneration in Glud1$^{\Delta Mo}$ mice is more efficient.

We then assessed how GLUD1-deficiency affects macrophage-mediated immunomodulation and vessel growth. Blood count, immune landscapes and vascular features of muscles at baseline and early after damage were similar in Glud1$^{\Delta Mo}$ *vs.* CTRL mice (Extended Data Table1; Extended Data Fig. 1o-w). *In vitro* and *in vivo* recruitment assays, macrophage polarization, as well as wound healing and angiogenic functions did not change (Extended Data Fig. 2a-e; Extended Data Fig. 3a-k). However, later after damage, total and M2-like macrophages were fewer in Glud1$^{\Delta Mo}$ *vs.* CTRL mice (Extended Data Fig. 3l,m), arguing that the faster resolution of inflammation is consequent to a more efficient muscle repair in Glud1$^{\Delta Mo}$ mice.

Metabolic changes within a cell affect the biology of neighbouring cells[18]. In WT macrophages, glutamine oxidation was 73% lower in glutamine-reduced *vs.* glutamine-enriched conditions (Fig. 2a). Compared to WT cells, glutamine oxidation in GLUD1 KO macrophages was lower in both culture conditions (Fig. 2a). However, total 2-oxoglutarate (2-OG) was comparable (Extended Data Fig. 4a), likely due to enhanced pyruvate carboxylase (PC)-dependent TCA-cycle anaplerosis (Fig. 2b), which compensates for the loss of glutamine-derived carbons[19]. Total energy charge, ATP production, ATP-linked oxygen consumption rate (OCR) were comparable in both genotypes (Extended Data Fig. 4b-d).

Though glutamine oxidation in GLUD1 KO macrophages was diminished, intracellular and extracellular glutamine production was higher under both glutamine-replete and, to a greater extent, glutamine-restricted conditions (Extended Data Fig. 4e,f). This was due to enhanced GS activity (Fig. 2c,d). At the protein level, GS was induced in WT macrophages under low glutamine but this induction was stronger in GLUD1 KO macrophages (Fig. 2e).

Glutamine uptake and conversion into glutamate were similar in WT and GLUD1 KO macrophages (Extended Data Fig. 4g,h).

GLUD1 converts glutamate into 2-OG but also 2-OG into glutamate, the latter used by GS to generate glutamine[12]. Consistent with this function, GLUD1 protein levels in WT macrophages were also upregulated under low glutamine (while undetectable in GLUD1 KO macrophages) (Fig. 2f). Under glutamine starvation, glucose utilization for glutamate production was enhanced in WT macrophages and even more in GLUD1 KO macrophages (Extended Data Fig. 4i,j). In absence of GLUD1, 2-OG into glutamate conversion was possibly taken-over by the increased activity of branched-chain amino acid aminotransferase (BCAT), utilizing branched-chain amino acids (leucine, isoleucine, and valine) as amino-group donors, or glutamate-oxaloacetate transaminase (GOT), utilizing aspartate (Fig. 2g). However, only the silencing of cytosolic BCAT (BCAT1) restored glutamine production by GLUD1 KO macrophages back to the WT levels (Extended Data Fig. 4k-n). Consistently, the BCAT1 inhibitor gabapentin prevented SC expansion in CTX-treated Glud1$^{\Delta Mo}$ mice (Extended Data Fig. 4o).

To assess the fate of macrophage-derived glutamine, we used a two-chamber co-culture of C2C12 myoblasts and macrophages in medium containing exclusively [$^{13}C_{5,}{}^{15}N_2$]-glutamine, *i.e.* glutamine labelled in the two nitrogen groups and in the five carbons. Uptake of [$^{13}C_5{}^{15}N_2$]-glutamine by myoblasts did not change in all the conditions (Fig. 2h). However, compared to myoblasts alone, intracellular total glutamine (labelled and unlabelled) was lower in myoblasts cultured with WT macrophages but higher in myoblasts cultured with GLUD1 KO macrophages (Fig. 2h). In macrophages, total glutamine levels were always higher in GLUD1 KO macrophages (Fig. 2i) though a comparable uptake in all the conditions (Fig. 2i). Since in myoblasts, the contribution to the total glutamine pool of [$^{13}C_{0,}{}^{15}N_0$]-

glutamine (derived from different sources than [$^{13}C_5$,$^{15}N_2$]-glutamine) was higher in co-culture with macrophages and peaked with GLUD1 KO macrophages (Fig. 2j), we argued that glutamine production by GLUD1 KO macrophages (Fig. 2j) outcompete glutamine consumption, increasing glutamine availability for myoblasts.

In vivo, interstitial glutamine levels in CTRL and Glud1$^{\Delta Mo}$ muscles were similar at baseline and dropped in injured CTRL but not in Glud1$^{\Delta Mo}$ muscles (Fig. 2k,l), whereas glutamate availability did not change (Extended Data Fig. 4p,q). GS depletion in macrophages worsened this post-injury glutamine shortage observed in control muscles, and also, disabled the preservation in glutamine levels seen in Glud1$^{\Delta Mo}$ muscles (Fig. 2m). Similarly, macrophage-specific depletion of GS worsened SC proliferation and muscle healing after injury, and it impeded the faster SC activation and damage resolution seen in Glud1$^{\Delta Mo}$ mice (Fig. 2n,o). Thus, macrophage GS is instrumental to replenish glutamine and promote SC activation in response to muscle damage (*i.e.* a glutamine-restricted condition).

Consistent with the above data, WT BMDMs placed in low glutamine showed reduced conversion of glutamate into 2-OG, a readout of oxidative GLUD1 activity (Extended Data Fig. 4r), whereas glutamine production involving the conversion of 2-OG into glutamate and glutamate into glutamine were both enhanced (Extended Data Fig. 4s,t). In muscle-infiltrating WT macrophages too, GS and oxidative GLUD1 activities, respectively, were gradually increasing and decreasing over time upon damage (Fig. 2p, upper panel), resulting in a slow increase of interstitial glutamine (Fig. 2p, lower panel). Muscle-infiltrating GLUD1 KO macrophages had constitutively inactive GLUD1 and higher GS activity (Extended Data Fig. 4u,v) which prevented the post-damage drop in interstitial glutamine (Fig. 2k).

We then linked macrophage-derived glutamine and myogenic potential. Myotube formation was promoted when differentiating C2C12 myoblasts were cultured in a glutamine-rich

151 medium and reduced under glutamine restriction (Fig. 2q,r). Co-culture of C2C12 cells with
152 WT macrophages impaired myogenic differentiation in glutamine-enriched conditions,
153 phenocopying a condition of low glutamine. Instead, co-culture of C2C12 cells with GLUD1
154 KO macrophages resulted in larger myotubes, regardless of glutamine availability in the
155 medium (Fig. 2q,r). Similar results were obtained with macrophage-conditioned media
156 (Extended Data Fig. 5a,b). SLC1A5 knockdown (KD) in C2C12 cells impaired glutamine uptake
157 (Extended Data Fig. 5c,d) and abrogated the advantage offered by GLUD1 KO macrophages
158 on myoblast differentiation (Extended Data Fig. 5e,f). Conditioned media from GLUD1 KO
159 macrophages enhanced the expression of both the proliferation marker *Pcna* and the
160 differentiation marker *Myogenin* and activated mTOR pathway (an important player for SC
161 proliferation/differentiation[20,21]) in a glutamine-uptake-dependent manner[22] (Extended
162 Data Fig. 5g,h). The mTOR inhibitor Torin2 abolished *Pcna* and *Myogenin* induction in C2C12
163 cells stimulated with conditioned media from GLUD1 KO macrophages (Extended Data Fig.
164 5g,h). Likewise, mTOR pathway was enhanced in SC isolated from CTX-injected Glud1$^{\Delta Mo}$ *vs.*
165 CTRL muscles (Fig. 2s).
166 In glutamine-replete conditions, SLC1A5-KD SC had impaired *in vitro*
167 proliferation/differentiation (Extended Data Fig. 5i-o). Therefore, to disrupt SLC1A5-
168 mediated glutamine import specifically in SC *in vivo*, AAV8 particles containing the gRNA
169 against *Slc1a5* were injected intramuscularly in LSL-Cas9/PAX7:Cre-ERT mice, carrying a
170 tamoxifen-inducible Cas9 in Pax7^{+} cells (Extended Data Fig. 6a-d). In this way SLC1A5 was
171 selectively knocked-down by 60% in about all the SC (Extended Data Fig. 6e-h). Using bone
172 marrow (BM) transplantation experiments, we confirmed that GLUD1 KO macrophages
173 ameliorated muscle regeneration in mice with SC proficient in glutamine uptake (non-
174 targeting control gRNA). Specifically, we administered EdU within 24h post-CTX and

collected the injured TA muscles 6 days post-CTX. Compared to muscles in Glud1^{WT} BM (CTRL BM), those from Glud1$^{\Delta Mo}$ BM mice treated with the non-targeting gRNA displayed a higher number of EdU^{+} terminally-differentiating myonuclei, increased MyoD^{+} myoblasts, higher number of Myogenin^{+} cells incorporated into the myofibers, as well as an increased area of regenerating myofibers (Fig. 2t-x). Conversely, when SC were perturbed in their capacity to import glutamine (*Slc1a5*-targeting gRNA), the superior myogenic potential of Glud1$^{\Delta Mo}$ BM mice was abrogated but also severely affected in Glud1^{WT} BM (CTRL BM) mice (Fig. 2t-x).

Mirroring muscle regeneration, tissue damage was milder in Glud1$^{\Delta Mo}$ BM mice treated with the non-targeting gRNA, but worsened by the *Slc1a5* gRNA in both CTRL and Glud1$^{\Delta Mo}$ BM mice (Fig. 2y, Extended Data Fig. 7a-d). As the maximal SC expansion in a WT context occurs between day 2 and day 4 post-CTX[23] (Fig. 1r), we administered EdU until day 3. In this setting, the number of EdU^{+} myonuclei was much higher compared to a 24h EdU pulse and anyhow strongly reduced when SC were deleted for the glutamine transporter *Slc1a5* (Extended Data Fig. 7e,f). Next to this approach, the SLC1A5 inhibitor gamma-L-Glutamyl-p-Nitroanilide (GPNA) impaired SC proliferation in both CTX-treated Glud1$^{\Delta Mo}$ and WT mice (Fig. 2z; Extended Data Fig. 5d). In sum, macrophage-derived glutamine uptake by SC plays a relevant role in the control of myogenic functions. Disrupting this cross-talk precludes the faster muscle repair in Glud1$^{\Delta Mo}$ mice but also delays muscle regeneration in CTRL mice.

Regenerative functions are known to decline with aging[24]. Muscle weight index in 18 month-old CTRL mice was reduced when compared to young mice, but this drop was less severe in Glud1$^{\Delta Mo}$ mice (Fig. 3a), as also indicated by the presence of larger myofibers (Fig. 3b,c). Interstitial glutamine followed the same trends (Fig. 3d). Fibrosis and macrophage infiltration were exacerbated in old *vs.* young CTRL mice, but to a lesser extent in Glud1$^{\Delta Mo}$

mice (Fig. 3e-g; Extended Data Fig. 8a), arguing that chronic inflammation inversely correlates with muscle health. Macrophage density in other tissues did not change (Extended Data Fig. 8b-i). Overall, muscle performance of 18 month-old Glud1$^{\Delta Mo}$ mice was better than age-matched CTRL mice (Fig. 3h-j). In line with this, Glud1$^{\Delta Mo}$ muscles displayed increased numbers but decreased ratio of phospho-p38 positive *vs.* negative SC (Fig. 3k-m), suggesting that SC self-renewal was better preserved in Glud1$^{\Delta Mo}$ mice[25].

We finally assessed the potential therapeutic effect of the GLUD1 inhibitor R162[26]. In response to CTX or ischemia, R162 treatment reduced muscle necrosis and inflammation (Fig. 3n-p), and boosted SC proliferation and interstitial glutamine concentration (Fig. 3q,r). In 18 month-old mice as well, administration of R162 for a month increased muscle mass, SC numbers, and interstitial glutamine, and improved physical performance (Fig. 3s-w). R162 did not affect body and organs' weights (Extended Data Fig. 8j-n).

This therapeutic benefit was selective for GLUD1 targeting. Unlike GLUD1 deletion (Extended Data Fig. 4g), macrophage-specific knockout of glutaminase (GLS), converting glutamine into glutamate, resulted in reduced glutamine uptake, glutamine oxidation, and 2-OG-to-succinate ratio but did not promote GS activity (Extended Data Fig. 9a-e). Six days post-CTX, interstitial glutamine levels, muscle damage, and macrophage infiltration were comparable in CTRL and Gls$^{\Delta Mo}$ mice, but macrophages were more M1-like in Gls$^{\Delta Mo}$ mice (Extended Data Fig. 9f-m), consistent with *in vitro* data (Extended Data Fig. 9n-q) and previous findings[27].

Muscle tissue is a major site for glutamine synthesis in the body[9,10,11]. We show here that muscle damage and aging restrain glutamine availability. Muscle-infiltrating macrophages sense this shortage and tilt down glutamine oxidation in favor of glutamine production. Macrophage-released glutamine is uptaken by SC promoting their proliferation and

differentiation through mTOR activation. Unlike WT macrophages, GLUD1 KO macrophages are pre-adapted to glutamine starvation, which results in improved regeneration (Extended Data Fig. 9r). Thus, a metabolic rewiring in macrophages re-establishes muscle homeostasis in response to damage.

The risk of vascular occlusion and skeletal muscle impairment is increased in case of diabetes, hypercholesterolemia, and obesity, which are recurrent in today's society[28]. Similarly, sarcopenic patients are arising together with the population age[29]. However, little can be done to improve these conditions[28,30]. Our data suggest a pharmacologic approach to treat damage and age-related skeletal muscle decline.

References

1 Bentzinger, C. F., Wang, Y. X., Dumont, N. A. & Rudnicki, M. A. Cellular dynamics in the muscle satellite cell niche. *EMBO reports* **14**, 1062-1072 (2013).

2 Costamagna, D., Berardi, E., Ceccarelli, G. & Sampaolesi, M. Adult Stem Cells and Skeletal Muscle Regeneration. *Current gene therapy* **15**, 348-363 (2015).

3 Saclier, M., Cuvellier, S., Magnan, M., Mounier, R. & Chazaud, B. Monocyte/macrophage interactions with myogenic precursor cells during skeletal muscle regeneration. *Febs J* **280**, 4118-4130 (2013).

4 Saclier, M. *et al.* Differentially activated macrophages orchestrate myogenic precursor cell fate during human skeletal muscle regeneration. *Stem cells* **31**, 384-396 (2013).

5 Tidball, J. G. Regulation of muscle growth and regeneration by the immune system. *Nature reviews. Immunology* **17**, 165-178 (2017).

6 Perdiguero, E. *et al.* p38/MKP-1-regulated AKT coordinates macrophage transitions and resolution of inflammation during tissue repair. *J Cell Biol* **195**, 307-322 (2011).

7 Latroche, C. *et al.* Coupling between Myogenesis and Angiogenesis during Skeletal Muscle Regeneration Is Stimulated by Restorative Macrophages. *Stem cell reports* **9**, 2018-2033 (2017).

8 Summan, M. *et al.* Macrophages and skeletal muscle regeneration: a clodronate-containing liposome depletion study. *American journal of physiology. Regulatory, integrative and comparative physiology* **290**, R1488-1495 (2006).

9 Rennie, M. J. *et al.* Skeletal muscle glutamine transport, intramuscular glutamine concentration, and muscle-protein turnover. *Metabolism: clinical and experimental* **38**, 47-51 (1989).

10 Biolo, G., Fleming, R. Y., Maggi, S. P. & Wolfe, R. R. Transmembrane transport and intracellular kinetics of amino acids in human skeletal muscle. *Am J Physiol* **268**, E75-84 (1995).

11 Nurjhan, N. *et al.* Glutamine: a major gluconeogenic precursor and vehicle for interorgan carbon transport in man. *J Clin Invest* **95**, 272-277 (1995).

12 Palmieri, E. M. *et al.* Pharmacologic or Genetic Targeting of Glutamine Synthetase Skews Macrophages toward an M1-like Phenotype and Inhibits Tumor Metastasis. *Cell Rep* **20**, 1654-1666 (2017).

13 St Pierre, B. A. & Tidball, J. G. Differential response of macrophage subpopulations to soleus muscle reloading after rat hindlimb suspension. *J Appl Physiol (1985)* **77**, 290-297 (1994).

14 Guardiola, O. *et al.* Induction of Acute Skeletal Muscle Regeneration by Cardiotoxin Injection. *Journal of visualized experiments : JoVE*, doi:10.3791/54515 (2017).

15 Takeda, Y. *et al.* Macrophage skewing by Phd2 haplodeficiency prevents ischaemia by inducing arteriogenesis. *Nature* **479**, 122-126 (2011).

16 von Maltzahn, J., Jones, A. E., Parks, R. J. & Rudnicki, M. A. Pax7 is critical for the normal function of satellite cells in adult skeletal muscle. *Proc Natl Acad Sci U S A* **110**, 16474-16479 (2013).

17 Zammit, P. S. Function of the myogenic regulatory factors Myf5, MyoD, Myogenin and MRF4 in skeletal muscle, satellite cells and regenerative myogenesis. *Semin Cell Dev Biol* **72**, 19-32 (2017).
18 Wenes, M. *et al.* Macrophage Metabolism Controls Tumor Blood Vessel Morphogenesis and Metastasis. *Cell metabolism* **24**, 701-715 (2016).
19 Yang, C. *et al.* Glutamine oxidation maintains the TCA cycle and cell survival during impaired mitochondrial pyruvate transport. *Mol Cell* **56**, 414-424 (2014).
20 Rodgers, J. T. *et al.* mTORC1 controls the adaptive transition of quiescent stem cells from G0 to G(Alert). *Nature* **510**, 393-396 (2014).
21 Zhang, P. *et al.* mTOR is necessary for proper satellite cell activity and skeletal muscle regeneration. *Biochem Bioph Res Co* **463**, 102-108 (2015).
22 Jewell, J. L. *et al.* Metabolism. Differential regulation of mTORC1 by leucine and glutamine. *Science* **347**, 194-198 (2015).
23 Rayagiri, S. S. *et al.* Basal lamina remodeling at the skeletal muscle stem cell niche mediates stem cell self-renewal. *Nat Commun* **9**, 1075 (2018).
24 Sousa-Victor, P. *et al.* Geriatric muscle stem cells switch reversible quiescence into senescence. *Nature* **506**, 316-321 (2014).
25 Bernet, J. D. *et al.* p38 MAPK signaling underlies a cell-autonomous loss of stem cell self-renewal in skeletal muscle of aged mice. *Nat Med* **20**, 265-271 (2014).
26 Jin, L. *et al.* Glutamate dehydrogenase 1 signals through antioxidant glutathione peroxidase 1 to regulate redox homeostasis and tumor growth. *Cancer cell* **27**, 257-270 (2015).
27 Liu, P. S. *et al.* alpha-ketoglutarate orchestrates macrophage activation through metabolic and epigenetic reprogramming. *Nature immunology* **18**, 985-994 (2017).
28 Obara, H., Matsubara, K. & Kitagawa, Y. Acute Limb Ischemia. *Ann Vasc Dis* **11**, 443-448 (2018).
29 Sayer, A. A. *et al.* New horizons in the pathogenesis, diagnosis and management of sarcopenia. *Age Ageing* **42**, 145-150 (2013).
30 Vinciguerra, M., Musaro, A. & Rosenthal, N. Regulation of muscle atrophy in aging and disease. *Adv Exp Med Biol* **694**, 211-233 (2010).

FIGURE LEGENDS

Figure 1| GLUD1 loss in macrophages boosts SC activation and muscle regeneration.
a-d, Post-CTX muscle necrosis (Baseline,B. *n*=4; Day1 *n*=4,6 CTRL,Glud1$^{\Delta Mo}$, respectively; Day6 *n*=10) (**a**) and regeneration (B. *n*=4,5; Day1 *n*=5,6; Day2 *n*=4; Day3 *n*=5; Day6 *n*=10) (**b**), with micrographs of H&E-stainings at Day6 showing necrotic (black-dotted line) (**c**) or regenerating (yellow-dotted line) fibers (**d**). **e,f,** Post-ligation necrosis (**e**) and regenerating area (**f**) 14 days post-ligation (B. *n*=4; Day1 *n*=5,4; Day3 *n*=7,8; Day14 *n*=9,6). **g-i,** Post-CTX muscle apoptosis by TUNEL staining (B. *n*=3; Day1 *n*=6; Day6 *n*=8) (**g**), with micrographs of Day6 (**h**), or post-ligation (B. *n*=3; Day1 *n*=4,5; Day3 *n*=5,3; Day14 *n*=4,3) (**i**). **j,** Oxidative stress by DHE stainings 6 days post-CTX or 14 days post-ligation (*n*=4). **k-m,** F/480^{+} macrophage infiltration post-CTX (B. *n*=4; Day1 *n*=4; Day6 *n*=10) (**k**), with micrographs of Day6 (**l**), or post-ligation (B. *n*=2; Day1 *n*=5; Day3 *n*=6; Day14 *n*=5,3) (**m**). **n,** Muscle viability (TTC staining) 6 days post-CTX (*n*=4). **o,p,** eMyHC^{+} myofibers (left) and eMyHC^{-} regenerating myofibers area (right) over cross-section area 6 days post-CTX (*n*=3) (**o**) and representative micrographs (**p**). **q,** Voluntary running (*n*=5). **r,s,** RT-qPCR on muscle extracts for Pax7 (B./Day1/Day3 *n*=6; Day6 *n*=4; Day10 *n*=4) (**r**) and *Myogenin* (B./Day1 *n*=6; Day3 *n*=8; Day6 *n*=6,4; Day10 *n*=4) (**s**). **t,u** Quiescent (PHH3^{-}) and proliferating (PHH3^{+}) SC at baseline and 1 day post-CTX (*n*=4,6), with representative micrographs (**t**), or 3 days post-ligation (*n*=4) (**u**). White arrows indicate Pax7^{+} or Pax7^{+}/PHH3^{+} cells; yellow arrows, Pax7^{+}/PHH3^{-} cells. **v-x,** WB on muscle extracts and densitometry for Pax7 (**v**), MyoD (**w**), Myogenin (**x**). A representative (**a-u,w,x**) or a pool (**v**) of at least two independent experiments is shown. Unpaired two-tailed *t*-test everywhere applied except in **q** (two-way ANOVA); ns, not significant. Bars: 10 µm (**h**), 20 µm (**c, l**), 50 µm (**d, p, t**). Graphs: mean ± SEM.

Figure 2| Uptake of macrophage-derived glutamine by SC boosts muscle regeneration.
a,b, Glutamine oxidation (*n*=3,4 WT,KO, respectively) (**a**), pyruvate-carboxylase activity (*n*=3) (**b**) in BMDMs under glutamine (Q)-enriched and Q-reduced conditions (*n*=4,3). **c,d,** Intra- and extracellular glutamine production (*n*=3) (**c**) and glutamine release under MSO-mediated GS inhibition (*n*=3) (**d**) in Q-starved BMDMs. **e,f,** WB and densitometry for GS (**e**) and GLUD1 (**f**) in BMDMs. **g,** BCAT, GOT, ALT activities in Q-starved BMDMs (*n*=3). **h-j,** Total glutamine, [$^{13}C_{5,}{}^{15}N_2$]-glutamine, [$^{13}C_0{}^{15}N_0$]-glutamine in C2C12 cells (**h,j**) and BMDMs (**i,j**), seeded alone or co-cultured in [$^{13}C_5$,$^{15}N_2$]-glutamine-containing medium (*n*=3). **k,l,** Interstitial glutamine 1 day post-CTX (Baseline,B. *n*=5,4 CTRL,Glud1$^{\Delta Mo}$, respectively; CTX *n*=9,8) (**k**) or 3 days post-ligation (B. *n*=7,9; ischemia *n*=12) (**l**). **m-o,** Interstitial glutamine and SC proliferation 1 day post-CTX (**m**,**n**), necrosis 6 days post-CTX (**o**) upon macrophagic GS

deletion (Glud1^{WT}GS^{WT} *n*=14,6,9 in **m**, **n**, **o**, respectively; Glud1$^{\Delta Mo}$GS^{WT} *n*=6,4,6; Glud1^{WT}GS$^{\Delta Mo}$ *n*=8,5,5; Glud1$^{\Delta Mo}$GS$^{\Delta Mo}$ *n*=8,5,8). **p,** Glutamate-to-2-OG (GLUD1 activity) and glutamate-to-glutamine (GS activity) conversion in muscle-infiltrating WT macrophages (upper panel) and interstitial glutamine in WT muscles (lower panel) (*n*=4). **q,r,** C2C12 myotubes in co-culture with BMDMs (*n*=3). **s,** WB and densitometry for phospho-P70S6K (1 day post-CTX) and phospho-S6 (3 days post-CTX) in isolated SC. **t-y,** Micrographs (**t**) and quantifications (n=4) of EdU^{+} myonuclei (**u**), MyoD^{+} nuclei (**v**), myoblast fusion (**w**), regenerating myofiber area (**x**), necrosis (**y**) 6-day post-CTX in mice reconstituted with GLUD1-WT (CTRL BM) or GLUD1-KO (Glud1$^{\Delta Mo}$) bone marrows (BM), and knocked-down (KD) or not (Ctrl gRNA) for SLC1A5 in SC. **z,** PHH3^{+} SC 1 day post-CTX after GPNA-mediated SLC1A5 inhibition (*n*=6,6,6,5 from right to left). A representative (**a-d,g-j,p-r,t-z**) or a pool (**e,f,k-o,s**) of at least two independent experiments is shown. Unpaired two-tailed *t*-test everywhere applied; ns, not significant; a.u., arbitrary units. Bars: 20 µm (**t**), 50 µm (**q**). Graphs: mean ± SEM.

Figure 3| GLUD1 loss or inhibition in macrophages benefits damaged and aged muscles.
a, Gastrocnemius weight (young mice *n*=8; aged mice *n*=6,9 CTRL,Glud1$^{\Delta Mo}$, respectively). **b,c,** Quantification (**b**) and micrographs (**c**) of fiber area in H&E-stained gastrocnemius sections (aged mice *n*=6). **d**, Intra-TA interstitial glutamine (young mice *n*=5,4; aged mice *n*=8). **e,f,** Quantification (**e**) for collagen deposition (in blue) in crural muscles of aged mice (*n*=7,8) on Masson's trichrome stainings (**f**). **g**, Macrophage infiltration in crural muscles of young or aged mice (*n*=8). **h-j,** Grip strength (*n*=5) (**h**), rotarod test (*n*=5) (**i**)**,** voluntary running (*n*=7,6) (**j**) in aged mice. **k,** Intra-TA SC density (*n*=5,7). **l-m** Pax7 and phospho-P38 in SC, associated to myofibers isolated from extensor digitorum longus muscles of aged mice (*n*=4). **n,o,** Muscle necrosis 6 days post-CTX (*n*=10) or 14 days post-ligation (*n*=5) upon R162-mediated GLUD1 inhibition (**n**), and micrographs showing ischemic necrosis (**o**). **p,** Macrophage infiltration 6 days post-CTX (*n*=10) or 14 days post-ligation (*n*=5). **q,** PHH3$^{+/-}$ SC 1 day post-CTX (*n*=5,6). **r,** Interstitial glutamine 1 day post-CTX (*n*=4,6). **s-w,** Gastrocnemius weight (*n*=6,7) (**s**), SC number per isolated TA myofiber (*n*=6,7) (**t**)**,** interstitial glutamine (*n*=11,14) (**u**), rotarod (*n*=7) (**v**) and grip strength test (*n*=7,8) (**w**) in vehicle and R162-treated aged mice. A representative of at least two independent experiments is shown in **a-r**. Unpaired two-tailed *t*-test everywhere applied except in **v** and **w** (two-way ANOVA); ns, not significant. Scale bars: 20 µm (**c, f, m, o**). Graphs: mean ± SEM.

METHODS

Mouse models: GLUD1 (*Glud1*$^{tm1.1Pma}$, MGI:3835667)[31], GS (*Glul*^{tm3Whla}, MGI:4462791)[32], GLS (*Gls*$^{tm2.1Sray}$, MGI:95752)[33] floxed mouse lines, all in a C57BL/6 background, were obtained respectively from Dr. Pierre Maechler (University of Geneva, Switzerland), Dr. Wouter H. Lamers (Academic Medical Center, Amsterdam, Netherlands) and Dr. Stephen Rayport (Columbia University, NY, US). *Glud1*$^{L/L}$;CSF1R:Cre-ERT transgenic mice were generated by intercrossing *Glud1* floxed mice with the tamoxifen-inducible, macrophage-specific CSF1R:Cre-ERT deleter mouse line (a gift of Dr. Jeffrey Dr. W. Pollard, University of Edinburgh, UK). PAX7:Cre-ERT transgenic mice[34], harboring a tamoxifen-inducible Cre under the Pax7 promoter for SC-specific expression, were provided by Dr. Katrien De Bock (ETH, Switzerland). LoxP-STOP-LoxP Cas9 mice (B6J.129(B6N)- Gt(ROSA) 26Sortm1(CAG-cas9*,-EGFP)Fezh/J)[35] were purchased from Jackson Laboratory. LSL-Cas9 x PAX7:Cre-ERT transgenic mice, a strain that has inducible Cas9 expression in germline under the SC-specific Pax7 promoter, were generated by intercrossing LoxP-STOP-LoxP Cas9 mice with PAX7:Cre-ERT transgenic mice line. Acute deletion of *Glud1* in macrophages was obtained by daily intraperitoneal (i.p.) injection of tamoxifen (0.05 mg per gram of body weight) for 5 days before and during cardiotoxin (CTX) (Latoxan) induced injury. Control mice were treated with tamoxifen according to the same protocol. All mice used for ischemia and CTX experiments were on a C57BL/6 background between 8 and 15 weeks old, while 18-month old mice were used for the aging experiments. Mice were used without specific gender selection. In all experiments, littermate controls were used. Housing and all experimental

448 animal procedures were approved by the Institutional Animal Care and Research Advisory
449 Committee of the KU Leuven.
450 **Cardiotoxin muscle injury:** Mice were anaesthetized with isoflurane and 50 µl of 10 µM CTX
451 was injected in the *tibialis anterior* (TA) muscle[14]. Control mice (denoted as baseline) were
452 subjected to PBS injection. For SC isolation, mice were injected with 50 µl of 10 µM CTX in
453 TA and 100 µl of 10 µM CTX in gastrocnemius muscles. Muscles were harvested for analysis
454 at different time points post-injury. *In vivo* GLUD1 inhibition was achieved by bi-daily gavage
455 of R162 (Focus Biomolecules) at 0.6 mg/mouse. Mice were pretreated 1 day before CTX
456 injection. Afterwards, mice continued to receive bi-daily treatment until their sacrifice. To
457 inhibit SLC1A5, mice were treated by oral gavage 3 times per day with a solution (200
458 µl/mouse) containing 500 mM GPNA (Sigma-Aldrich). CTX was injected 1 h after the first
459 gavage, and mice were sacrificed 24 h afterwards. *In vivo* BCAT1 inhibition was achieved by
460 bi-daily i.p. injection of gabapentin (Sigma-Aldrich) at 2 mg/mouse. Mice were pretreated
461 once before CTX injection, and mice were sacrificed 24 h afterwards.
462 **Hindlimb ischemia:** To induce acute hindlimb ischemia and greatly prevent flow redirection
463 into the collateral circulation, which leads to severe muscle necrosis, unilateral or bilateral
464 ligations of the high femoral artery were performed without damaging the nervus femoralis
465 as previously described[15]. Control mice (denoted as baseline) were subjected to a sham
466 operation that did not involve the ligation of the femoral artery. Functional perfusion
467 measurements were performed using a Lisca PIM II camera (Gambro)[15]. GLUD1 inhibition
468 was achieved by bi-daily gavage of R162 (Focus Biomolecules) at 0.6 mg/mouse. Mice were
469 pretreated 1 day before femoral artery ligation. Afterwards, mice continued to receive bi-
470 daily treatment until their sacrifice.

Wheel running test: Physical activity was assessed with voluntary wheel running test. Mice were individually housed in cages equipped with 12 cm diameter wheels for rodents, wheels were connected with cycle computers (SunDing SD-568AE). After 1 week of acclimatization, physical activity (*i.e.* duration, running speed, and distance) was recorded daily.

Rotarod test: Whole body mobility and coordination was assessed by rotarod performance. Following a 5 min acclimatization in the test room, mice were placed on the rod (Biological research apparatus), which was rotating at an initial speed of 4 rpm. The speed was increased gradually from 4 rpm to 40 rpm within 5 min and latency to fall on to a soft pad was recorded. The test was repeated twice more, with 15 min between tests. After 3 days training, latency to fall was calculated over 3 trials.

Grip test: Muscle strength was measured by pulling backwards the mice with a continuous movement when the mice were hold firmly to the grip of strength meter (Chatillon, DFE II Digital Force Gauge). The test was repeated twice more, with 15 min between tests. Results was calculated over the 3 trials.

TTC staining: TA muscles were collected 6 days after CTX injection. After scarification muscles were washed in PBS and cut in transversal sections. Sections were incubated with a buffered (pH 7.4) 1.5% 2,3,5- triphenyl-tetrazolium chloride (TTC) solution at a temperature of 37°C for 40 min. Pictures were taken with NIKON camera. The quantification was performed with Image J software. Images were converted in a grey scale and it was calculated the mean grey intensity of each section.

Interstitial fluid preparation: Intact TA muscles for the CTX model, or crural muscles (gastrocnemius and soleus muscles) for the ischemia model, were placed into test tubes with perforated bottom. 20 µL of 0.9% NaCl solution (pH 7.4) was added to the sample. Interstitial fluid was collected by centrifugation (110 g, 10 min, 4°C). Protein within the

interstitial fluid was precipitated using −20°C cold methanol/water-mix (5:3) and centrifuged (20000 x g, 5 min, 4°C). The supernatant was dried using a vacuum centrifuge and derivatized for mass spectrometry analysis.

Bone marrow transplantation: 5-6 weeks old recipient mice were irradiated with 9.2 Gy. Subsequently, $10x10^6$ bone marrow cells from the appropriate genotype were injected intravenously via the tail vein. Muscle injury experiments were initiated 5 weeks after bone marrow reconstitution. Red and white blood cell count was determined using a hemocytometer on peripheral blood collected in heparin with capillary pipettes by retro-orbital bleeding.

***In vitro* and *in vivo* targeting of the *Slc1a5* locus:** To generate *in vitro* a stable C2C12 mouse myoblast cell line and primary SC, deficient for SLC1A5, lentiCRISPRv2 vectors expressing the Cas9 along with a gRNA targeting the *Slc1a5* locus (AATCCCTATCGATTCCTGTG) or a non-taregting control gRNA (GAACAGTCGCGTTTGCGACT), were used. $2x10^4$ C2C12 cells/well were seeded in 12-well plates and transduced with purified lentiviral vectors in the presence of 8 µg/ml polybrene for 48 h. After adding virus, the plate was centrifuged for 30 min at 800x g, 25-32°C. Transduced cells were selected with puromycin (4 µg/ml) during a period of 5 to 7 days. The lentiCRISPRv2 was a gift from Dr. Feng Zhang (Addgene plasmid # 52961)[36]. The gRNAs were cloned as described previously[36]. For an optimal transduction of SCs cells *in vivo* and specifc targeting of the *Slc1a5* locus exclusively in SCs, the gRNAs described above were cloned in the AAV_Guide vector (see also Extended Data Fig. 6a). AAV8 production and titration was outsourced to Vigene Biosciences (Rockville, MD 208050, USA). Two-day-old (P2) neonatal LSL-Cas9 x PAX7:Cre-ERT transgenic mice were then administered locally into the TA muscles with 6.7 X 10^{10} vector genomes (vg) per injection (5 µl/leg). Bone marrow cells from CTRL and Glud1$^{\Delta Mo}$ mice were transplanted at the age of five weeks. Five weeks

after bone marrow reconstitution, tamoxifen was given by daily oral gavage for five days before and three days after CTX induced injury. 180 µg EdU was given by i.p. injection 24 h after CTX injection. 3 hours after CTX injection mice also received a second AAV injection into the TA muscles (4 X 10^{11} vg per injection, see shematic in Extended Data Fig. 6b).

SC isolation and culture conditions: Hindlimb muscles were dissected and minced in small fragments by scissors and digested in 0.1% collagenase/0.25% trypsin solution at 37°C with gentle shaking for 20 min as previously described[37]. Supernatants were collected in fetal bovine serum (FBS) at 37°C and passed through 40 µm filters. The digestion step was repeted 3 times until the complete dissociation of samples. The fraction of freshly isolated SC was enriched by using the SC isolation kit (Miltenyi Biotec, 130-104-268). SC were collected on glass slides by cytospin for immunofluorescence analyses, or snap frozen for protein extraction. The fraction of non-SC (Miltenyi Biotec, 130-104-268) was used as control where indicated.

SC were seeded on collagen-coated dishes (Sigma) and maintained in growth medium (GM), that, for SC, is DMEM (Gibco) supplemented with 20% FBS (Gibco), 10% Horse Serum (HS) (Gibco), 1% Chicken embryo extract (Seralab), 2 mM glutamine, 110 mg/ml sodium pyruvate (Gibco), 100 units/ml penicillin and 100 µg/mL streptomycin (Gibco), or in differentiation medium (DM), that is DMEM supplemented with 2% HS, 2 mM glutamine, 110 mg/ml sodium pyruvate, 100 units/ml penicillin and 100 µg/mL streptomycin.

EdU-based SC proliferation assays were performed by seeding in 6 well plates 3.0 × 10^4 cells/well in GM containing 10 µM of 5-ethylnyl-2'-deoxyuridine (EdU) (Thermo Fisher, C10337) for 24 h prior the fixation. Click-iT® reaction and staining were performed according to the manufacturer's instructions.

Differentiation assays were performed by seeding 1.0 x 10^4/cm^2 SC in GM. After 24 h, GM was replaced with DM for 5 days. Myotubes-derived SC were fixed in 4% paraformaldehyde and stained for myosin heavy chain. Fusion index (percentage of nuclei within myotubes: myotube=nuclei≥2) and myotube size (mean of number of nuclei into myotubes) were analyzed.

Single fiber isolation and immunostaining: Single myofibers were isolated from extensor digitorum longus (EDL) muscles of aged mice as previously described[37]. Briefly, intact muscles were dissected from tendon to tendon and digested with a solution containing 0.2% collagenase type I (Sigma) in DMEM (Dulbecco's modified Eagle's medium; high glucose, L-glutamine with 110 mg/ml sodium pyruvate) at 37°C for 3h. Afterward, individual fibers were separated from each others by pipetting under a dissecting microscope, and then washed in DMEM.

Fresh isolated fibers were fixed in 4% paraformaldehyde, 6min at RT, permeabilized by a solution containing 0.5% Triton, 8 min at RT, blocked with 20% HS 1h at RT and incubated overnight at 4°C with anti mouse pax7 (DHSB, 1:20) and anti rabbit Phospho-p38 MAPK (Cell Signaling Technology, 1:200) followed by incubation with anti rabbit Alexa 488, and anti mouse 568 conjugated secondary antibodies (Invitrogen, 1:1000). 28-30 fibers per point were analysed.

Cell lines: C2C12 murine myoblast cells were obtained from the American Type Culture Collection (ATCC). C2C12 authentication was confirmed by testing their myogenic differentiation capacity. Specifically, RT-qPCR and immunofluorescence analyses of the expression of specific myogenic markers (*e.g.* myogenin and myosin heavy chain) confirmed their myogenic origin. Cells were regularly tested for mycoplasma via PCR.

Glutamine-enriched and glutamine-reduced media preparation: When specified, the glutamine (Q)-enriched medium (4mM glutamine) was obtained by supplementing M199 or DMEM with 10% FBS. A glutamine (Q)-reduced medium (0.03 mM glutamine) was obtained by supplementing M199 or DMEM (with no glutamine) with 10% FBS, dialyzed for glutamine. Dyalized FBS was obtained by slide A lyzer dialysis cassette (Thermo Scientific 66130).

***In vitro* C2C12 co-cultures with BMDMs:** C2C12 cells were cultured in growth medium (GM), that for C2C12 cells, is DMEM (Gibco) supplemented with 10% FBS (Gibco), 2 mM glutamine, 100 units/ml penicillin and 100 µg/ml streptomycin. C2C12 myoblasts were cultured for no more than 6 passages in a humidified incubator in 5% CO_2 and 95% air at 37°C. To obtain BMDM-conditioned media (CM), 2 x 10^6 BMDMs (WT or GLUD1 KO) were cultured in a 6 cm dish for 48h in Q-enriched or Q-reduced medium.

In the proliferation assay, 6 x 10^4 C2C12 cells/well were seeded in 6-well plates in GM. After 24 h, regular GM was replaced with a Q-reduced GM that was previously conditioned by WT or GLUD1 BMDMs.

In the differentiation assay, 6 x 10^4 C2C12 cells/well were seeded in a 6-well plates in GM. After 24 h, GM was replaced with Q-enriched or Q-reduced differentiation medium (DM), that is the same medium as described above for SC. At day 2 of myoblast differentiation, 1.5 x 10^5 BMDMs or BMDM-conditioned DM were added to the differentiating myotubes for additional 4 days. Afterwards, samples were collected for RNA or fixed in 4% formaldehyde for 10 min at RT and permeabilized in PBS with 1% BSA, 0.2% TritonX for 30 min and blocked in 10% Donkey serum 1h at RT. Finally, samples were incubated overnight at 4°C with mouse anti-MF20 (DSHB, 2µg/ml) and subsequently incubated with AlexaFluor 568-conjugated

donkey anti-mouse (Invitrogen 1:1000). When indicated, mTOR inhibition was achieved by adding 500nM Torin2 (Selleck Chemicals) to the medium.

***In vitro* BMDM-C2C12 co-cultures with [^{13}C5^{15}N2]-glutamine:** 2.5 x 10^5 BMDMs were seeded in the top chambers of a 24-well transwell plate (0.4 µm polycarbonate membrane) whereas 1.5 x 10^5 C2C12 cells were seeded in the lower wells, in a medium where the only glutamine present was labelled in the two nitrogen groups and in the five carbons ([^{13}C5^{15}N2]-glutamine). After 48h, cells were scraped in 80% methanol and phase separation was achieved by centrifugation at 4°C. Methanol-water phase containing polar metabolites was separated and dried using a vacuum concentrator. The dried metabolite samples were stored at −80°C. Isotopomer distributions and metabolite levels were measured with a 7890A GC system (Agilent Technologies) combined with a 5975C Inert MS system (Agilent Technologies).

Glutamine oxidation: Each M199 media (Q-enriched or Q-reduced) was supplemented with 0.5 µCi/ml [U-^{14}C]-glutamine. After incubating 1 x 10^6 BMDMs in a 12-well plate for 6h, 250 µl of 2 M perchloric acid was added to each well to stop cellular metabolism. Each well was immediately covered with a 1 x hyamine hydroxide-saturated Whatman paper. Overnight absorption of $^{14}CO_2$ released during the oxidation of glutamine into the paper was performed at RT and radioactivity in the paper was determined by liquid scintillation counting.

Glutamine uptake: 2 x 10^6 BMDMs were seeded in a 6-well plate and cultured in M199 medium (Gibco) and 10% FBS, supplemented with 0.5 µCi/ml [U-^{14}C]- glutamine for 30 min at 37°C. Cells were lysed in 1N NaOH and the radioactivity was measured by liquid scintillation counting.

A(X)P detection by LC-MS: 2 x 10^6 BMDMs were lysed in 300 µl extraction buffer (50:30:20 mix of methanol:acetonitrile:10 mM Tris pH 9.3). Following extraction, samples were centrifuged for 10 min at 20000 x g (at 4°C). The supernatant was transferred to a vial. 35 µl was loaded onto an Ultimate 3000 UPLC (Thermo Scientific, Bremen, Germany) equipped with a ZIC-pHILIC column (2.1 x 150 mm, 5 µm particle size, cat# 1.50460.0001, Merck, Darmstadt, Germany) in line connected to a Q Exactive mass spectrometer (Thermo Fisher Scientific). A linear gradient was carried out starting with 90% solvent A and 10% solvent B. From 2 to 20 min the gradient changed to 80% B and was kept at 80% until 23 min. Next a decrease to 40% B was carried out to 25 min, further decreasing to 10% B at 27 min. Finally 10% B was maintained until 35 min. The solvent was used at a flow rate of 200 ul/min, the columns temperature was kept constant at 25°C. The mass spectrometer operated in negative ion mode, settings of the HESI probe were as follows: sheath gas flow rate at 35, auxiliary gas flow rate at 10 (at a temperature of 260°C). Spray voltage was set at 4.8 kV, temperature of the capillary at 300°C and S-lens RF level at 50. A full scan (resolution of 140.000 and scan range of m/z 70-1050) was applied. For the data analysis we used an in-house library and metabolites of interest were quantified (area under the curve) using the XCalibur 4.0 (Thermo Scientific) software platform. The energy charge was calculated as ([ATP]+1/2[ADP])/ ([ATP]+ [ADP] +[AMP]).

Oxygen consumption: 1.5 x 10^4 BMDMs were incubated overnight on Seahorse XF24 tissue culture plates (Agilent). During the assay, the medium was replaced by unbuffered DMEM supplemented with 5 mM D-glucose and 2 mM L-glutamine, pH 7.4. The measurement of oxygen consumption was performed at 6 min intervals (2min mixing, 2min recovery, 2min measuring) using the Seahorse XF24 analyzer. Inhibitors were serially injected at the

following concentrations: oligomycin (1 µM), FCCP (fluoro-carbonyl cyanide phenylhydrazone, 1.5 µM), antimycin A (1 µM) (all from Sigma-Aldrich).

^{13}C and ^{15}N tracing experiments: For ^{13}C and ^{15}N tracing experiments, cells were incubated with [U-^{13}C]-L-glutamine (2 mM), [U-^{13}C]-L-glutamate (0.25 mM), [U-^{13}C]-D-glucose (5 mM), $^{15}NH_4Cl$ (2 mM), [^{15}N, ^{13}C4]-aspartate (1 mM), [^{15}N, ^{13}C4]-alanine (1 mM) or [^{15}N]-leucine (0.8 mM) for 48 h (confirmation of steady state) respectively (all from Cambridge Isotope Laboratories).

Metabolites quantification by LC-MS/MS: For mass spectrometry analysis of glutamate and glutamine, 2×10^6 cell pellets were washed twice in PBS and extracted in 500 µl of 80% methanol. Upon extraction, samples were centrifuged at 20000 x g for 15 min and the supernatant was dried using a vacuum centrifuge. 25 µl of a 2% methoxyamine hydrochloride solution were added to the dried pellet and the tubes were then placed at 37°C for 90 min. Then 75 µl of N-tert-Butyldimethylsilyl-N-methyltrifluoroacetamide with 1% N-tert-Butyldimethyl-chlorosilane (Sigma-Aldrich, Bornem, Belgium) was added and the reaction was carried out for 30 min at 60°C. Reaction mixtures were then centrifuged for 15 min at 20000 g at 4°C in order to remove insolubilities, the supernatant was transferred to a glass vial with conical insert (Agilent). GC-MS analyses were performed using an Agilent 7890A GC equipped with a HP-5 ms 5% Phenyl Methyl Silox (30 m - 0.25 mm i.d. - 0.25 µm; Agilent Technologies, Santa Clara, California, USA) capillary column, interfaced with a triple quadruple tandem mass spectrometer (Agilent 7000B, Agilent Technologies) operating under ionization by electron impact at 70 eV. The injection port, interface and ion source temperatures were kept at 230°C. Temperature of the quadrupoles was maintained at 150°C. The injection volume was 1 µl, and samples were injected at 1:25 split ratio. Helium flow was kept constant at 1 ml/min. The GC oven temperature was held at 60°C for 3 min,

increased to 300°C at 9°C/min, and kept for 2 min. The mass spectrometer operated in SIM mode, glutamine and glutamate were determined from the *m/z* 341.2 and 342.2 respectively. For quantifications, the MassHunter Workstation Software B.06.00 SP01 (Agilent Technologies) was used.

***In vivo* GS activity and glutamate to 2-OG conversion:** GS activity and glutamate to 2-OG conversion in muscle-infiltrating macrophages, sorted 1 and 3 days after CTX injection, were measured respectively with the glutamine synthetase microplate assay kit (ABIN2704091, Cohesion Biosciences) and the glutamate dehydrogenase activity assay kit (MAK099-1KT, Sigma-Aldrich).

TPA model of acute skin inflammation: Phorbol ester TPA was used to induce acute skin inflammation as described before[38]. Briefly, TPA (2.5 µg in acetone, 20 µl total volume/site) was topically applied on the ear skin of anaesthetized mice. As vehicle control, the ear was painted with acetone alone. After the indicated time points, tissue was harvested for further analysis.

FACS analysis of muscle macrophages: TA muscles were dissected, dissociated mechanically, digested using 800U/ml collagenase II (10 ml per sample) for 1 h at 37°C, centrifuged and resuspended with 1000U/ml collagenase II (1 ml per sample) and 11U/ml Dispase (1 ml per sample) solution and incubated for 30 min at 37°C. The digested tissue was filtered using a 40 µm pore sized mesh and cells were centrifuged 5 min at 500 g. Cells were resuspended in FACS buffer (PBS containing 2% FBS and 2 mM EDTA), incubated for 15 min with Mouse BD Fc Block purified anti-mouse CD16/CD32 mAb (BD-pharmingen) and stained with the following antibodies for 30 min at 4°C: viability dye (Invitrogen), anti-CD45 (Biolegend), anti-CD11b (Invitrogen), anti-F4/80 (Invitrogen), anti-MHCII (Invitrogen), anti-CD80 (Invitrogen) and anti-CD206 (Biorad), anti-CD45R (BD Biosciences), anti-Ly6G (BD

682 Biosciences,), anti-TCRβ (BD Biosciences), anti-CD4 (BD Biosciences) and anti-CD8
683 (Invitrogen,). Cells were subsequently, washed and resuspended in cold FACS buffer before
684 FACS analysis or flow sorting by a FACS Verse or FACS Aria (BD Biosciences), respectively.
685 Fluorescence minus one (FMO) controls were performed in all the stainings and used for the
686 proper gating in all the analysis.
687 **Histology and immunostainings:** 7 μm-thick cryosections were obtained by using a Leica
688 cryostat from frozen muscles collected in optimal cutting temperature compound (OCT) and
689 fixed in 4% formaldehyde for 10 min at RT. Alternatively, TA and crural muscle were fixed in
690 2% paraformaldehyde, dehydrated, embedded in paraffin, and sectioned at 7 μm thickness.
691 Necrotic muscle area was detected by H&E staining as the area which includes necrotic
692 myocytes, inflammatory cells and interstitial cells. After deparaffinization and rehydration,
693 muscle sections were permeabilized by a solution containing 1% BSA, 0.2% Triton-X in PBS
694 30 min at RT, blocked with 10% Donkey serum (Sigma) 1 h at RT and treated with target
695 retrieval solution at pH 6.1 (Dako, S1699) at 92°C for 20 min. To reduce the immune
696 background sections were blocked with 10% donkey serum in PBS, 1h at RT, followed by
697 blocking with FAB fragment anti-mouse IgG (Jackson Immunoresearch, 1:5-1:10), 1h at RT
698 and 0.3% H_2O_2 in PBS for 30 min at RT to block endogenous peroxidase activity. Slides were
699 incubated overnight at 4°C with primary antibodies: rat anti-F4/80 (Bio-Rad, 1:100), rabbit
700 anti-laminin (Sigma-Aldrich, 1:300), rabbit anti-phospho-histone H3 (Millipore, 1:1000),
701 mouse anti-MF20 (DSHB, 2μg/ml), rabbit anti-Dystrophin (Abcam, 1:50), mouse anti-MyoD
702 (Santa Cruz, 1:10), mouse anti-embryonic Myosin (DSHB, 1:20), mouse anti-Myogenin
703 (DSHB, 1:1), mouse anti-Pax7 (DSHB, 1:20), rat anti-CD34 (BD Biosciences), mouse anti-
704 MMR/CD206 (R&D Systems, 1:100), rabbit anti-Ki67 (Abcam, 1:100), rabbit anti-CRISPR-Cas9
705 (Abcam, 1:500). Appropriate secondary antibodies were used: Alexa 488, or 568 conjugated

secondary antibodies (Invitrogen, 1:1000), biotin-labeled antibodies (Jackson Immunoresearch, 1:500-1:2000) and, when necessary, TSA fluorescein tyramide, TSA Plus Cyanine 3 or Cyanine 5 System amplification (Perkin Elmer, Life Sciences, 1:500-1:2000) were performed according to the manufacturer's instructions. Immunofluorescence of SC cytospinned on glass slides was performed by fixation in 4% formaldehyde for 10 min at RT, followed by incubation with 0.5% Triton-X in PBS for 20 min at RT and blocking with with 10% donkey serum for 1h at RT. Samples were then probed with mouse anti-Pax7 (DSHB, 1:20) alone or incombination with rabbit anti-SLC1A5 (Alomone Labs, 1:50) for 2h at RT followed by incubation with mouse Alexa 568 (Invitrogen, 1:10000), or a combination of mouse Alexa 488 and rabbit 568 conjugated secondary antibodies (Invitrogen, 1:1000), respectively. *In vivo* cell proliferation and differentiation was detected by DNA incorporation of thymidine analogue EdU (ThermoFisher, Click-iT C10337) in combination with Dystrophin staining on muscle cryosections. Oxidative damage was detected by dihydroethidium (DHE) (Life Technology). Samples were incubated with 10 μM DHE at 37°C for 30 min. Apoptosis was detected by TUNEL assay kit (Sigma-Aldrich) according to the manufacturer's instructions. Nuclei were counterstained with Hoechst-33342 (Invitrogen, 1:1000). Whenever sections were stained in fluorescence, ProLong Gold mounting medium with or without DAPI (Invitrogen) was used.

Imaging and Morphometry: Images were acquired by an Olympus BX41 microscope equipped with the CellSense Dimension imaging software. CellSense Dimension software was used for the morphometric analyses of cell cultures and muscle tissue. Myotubes diameter was measured as the average from three independent measurements per myotube.

Bone marrow-derived macrophages (BMDMs): Macrophages were derived from bone marrow precursors as described before[38]. Briefly, bone marrow cells (1.6 x 10^6 cells/ml) were cultured in a volume of 6 ml in a 10 cm Petri dish in DMEM supplemented with 20% FBS and 30% L929 conditioned medium as a source of M-CSF. After 3 days of culture, an additional 3 ml of differentiation medium was added. At day 7, macrophages were harvested with ice cold $Ca2^+$ and $Mg2^+$-free PBS. The cells obtained were uniformly macrophages as assessed by FACS, using the pan-macrophage marker F4/80. When indicated, GS inhibition in cultured BMDMs was achieved by adding 1 mM L-methionine-SR-sulfoximine (MSO; Sigma) to the medium for 48 h. Silencing of Bcat1, Bcat2, Got1, Got2 and Alt in BMDMs was achieved by electroporation with specific siRNAs (IDT). Briefly, 5.6 x10^6 BMDMs were resuspended in 750 µl of Opti-MEM and were electroporated (250V, 950 µF, ∞ Ω) with 120 pmol of total siRNA IDT. Control BMDMs were electroporated with scrambled siRNA sequences.

BMDM migration assay: Migration of BMDMs was assessed by using a 8-µm-pore Transwell permeable plate (Corning Life Science). The bottom chambers contained DMEM with specific chemoattractants or controls (specified in each Figure), BMDMs were harvested and then seeded in the upper chamber (2.5 x 10^5 cells in 200 µl of DMEM at 2% HS). After 4 h incubation, migrated cells were fixed with 4% paraformaldehyde, stained with 5mg/ml crystal violet/20% methanol and counted under the microscope.

Macrophage phagocytosis: BMDMs were treated with 50 ng/ml of IL-4 in DMEM complete, non-treated condition was used as control. 6 h after treatment, cells were harvested and incubated 40 min at 37°C with latex beads (1:5000) (Polysciences Ref. # 17152-10), negative controls were incubated 40 min at 4°C. After incubation, cells were washed with 2ml MACS buffer, and read by FACS in the FITC channel.

753 **Endothelial sprouts:** BMDMs were treated with 10 ng of IL-4 in DMEM complete, non-
754 treated condition was used as control. 24 h after treatment, macrophages were harvested
755 and incubated overnight with HUVECs (1400 BMDMs and 1400 HUVECs) in hanging drops of
756 25 µL in EGM-2 medium containing methylcellulose (methylcellulose 4000 cP, Sigma-Aldrich,
757 Bornem, Belgium) to form spheroids. Then, spheroids were harvested and embedded in
758 collagen type I gel in a 24-well plate and cultured for 20 h to induce sprouting. Spheroids
759 were fixed with 4% PFA and images were captured with a LEICA DM1600B inverted light
760 microscope. The total sprout length per spheroid (cumulative length of primary sprouts and
761 branches) was done manually using the Image J software.
762 **Protein extraction and immunoblot:** Whole cell protein extraction was performed using
763 extraction Buffer (20 mM Tris HCl, 150 mM NaCl, 1% Triton X-100, 10% glycerol, 5 mM
764 EDTA) supplemented with Complete Mini protease inhibitor (Roche) and PhosSTOP
765 Phosphatase Inhibitor (Roche). A protein load (from 15-40 µg) was separated by NuPAGE®
766 4-12% Bis-Tris (Thermofisher) or Any kD™ Mini-PROTEAN® TGX™ (Biorad) Precast Gels and
767 transferred electrophoretically to nitrocellulose membrane by iBlot System (Thermofisher).
768 Nonspecific binding was blocked in Tris-Cl Buffered Saline Solution with 0.05% Tween-20
769 (TBST) containing 10% non-fat dry milk or 5% of bovine serum albumin. The following
770 antibodies were used: GLUD1 (Abcam, 1:3000), GS (Sigma-Aldrich, 1:5000), Pax7 (DSHB,
771 0.5µg/ml), MyoD (Santa Cruz, 1:500), Myogenin (DSHB, 0.2µg/ml), phospho-p70S6K (Cell
772 signaling technology), p70S6K (Cell signaling technology, 1:1000), phospho-S6 ribosomal
773 protein (Cell signaling technology, 1:1000), S6 ribosomal protein (Cell signaling technology,
774 1:1000), Vinculin (Sigma-Aldrich, 1:1000), and appropriate HRP-conjugated secondary
775 antibodies (Cell signaling technology, 1:3000-1:10000). Signal was visualized by Enhanced
776 Chemiluminescent Reagents (ECL, Invitrogen) or West Femto by Thermo Scientific according

to the manufacturer's instructions and acquired by a LAS 4000 CCD camera with ImageQuant software (GE Healthcare). Densitometry was performed by using Image J software, expressing the data as percentage of the signal for the indicated protein *vs.* an house-keeping control or the phosphorylated form *vs.* its unphosphorylated total protein.

RT-qPCR: Cells were washed in PBS, collected in RLT buffer (Qiagen) and kept at -80°C. RNA was extracted with the RNeasy Micro kit (Qiagen) according to manufacturer's instructions. Reverse transcription to cDNA was performed with the SuperScript® III First Strand cDNA Synthesis Kit (Life Technologies) according to manufacturer's protocol. Pre-made assays were purchased from IDT (*Pax7*, Mm.PT.58.12398641; *Myogenin*, Mm.PT.58.6732917; *Pcna*, Mm.PT.58.33207367; *Cxcl9*, Mm.PT.58.5726745; *Tnfa,* Mm.PT.58.12575861; *Arg1*, Mm.PT.58.8651372; *Il10*, Mm.PT.58.13531087, *Mrc1*, Mm.PT.47.7673017; *Retnla*, Mm.PT.58.43062398; *Glud1*, Mm.PT.58.43368019; *Hprt*, Mm.PT.58.32092191; *Slc1a5*, Mm.PT.58.33492914). cDNA, primer/probe mix and TaqMan Fast Universal PCR Master Mix were prepared in 10 µl according to manufacturer's instructions (Applied Biosystems). Samples were loaded into an optical 96-well Fast Thermal Cycling plate (Applied Biosystems) and RT-qPCR were performed using an ABI Prism 7500 Fast Real-Time PCR System (Applied Biosystems). To detect genome editing (indel) of the *Slc1a5* target locus at transcriptional level, we designed a spefic primer set. The forward primer 5'- AATCCCTATCGATTCCTGTGG -3' anneals to the gRNA cutting site whereas, the reverse primer 5'-GAACCGGCTGATGTGTTTGG -3' anneals to a non-targeted coding region. Thus, mutations of the gRNA target site will disrupt the amplification of the target region. cDNA, primers and PowerUp SYBR Green Master Mix were prepared in a volume of 20 µl according to manufacturer's instructions (Applied Biosystems).

RNA sequencing: RNA concentration and purity were determined spectrophotometrically using the Nanodrop ND-1000 (Nanodrop Technologies) and RNA integrity was assessed using a Bioanalyser 2100 (Agilent). Per sample, an amount of 4 ng of total RNA was used as input for the SMART-Seq v4 Ultra Low Input RNA protocol (version "091817") from Takara Bio USA, Inc. Subsequently, 5 ng of purified cDNA was sheared to 300bp using the Covaris M220. From the sheared material, sequencing libraries were prepared with the NEBNext Ultra DNA Library Prep Kit for Illumina (version 6.0 -2/18), according to the manufacturer's protocol including a size selection to 250bp insert size. Sequence-libraries of each sample were finally equimolarly pooled and sequenced on 1 NextSeq500 v2 flow-cell at 1x75 bp (76-6-0-0).

Statistics: Data entry and all analyses were performed in a blinded fashion. All statistical analyses were performed using GraphPad Prism software on mean values calculated from the averages of technical replicates. Statistical significance was calculated by two-tailed unpaired t-test on two experimental conditions or two-way ANOVA when repeated measures were compared, with $P<0.05$ considered statistically significant. The exact P values are always reported except when $P<0.0001$. No values were excluded from the analyses. Sample sizes for all experiments were chosen based on previous experiences. Independent experiments were pooled and analyzed together whenever possible as detailed in figure legends. All graphs show mean values ± standard error of the mean (SEM).

31 Carobbio, S. *et al.* Deletion of glutamate dehydrogenase in beta-cells abolishes part of the insulin secretory response not required for glucose homeostasis. *J Biol Chem* **284**, 921-929 (2009).
32 He, Y. *et al.* Glutamine synthetase deficiency in murine astrocytes results in neonatal death. *Glia* **58**, 741-754 (2010).
33 Mingote, S. *et al.* Genetic Pharmacotherapy as an Early CNS Drug Development Strategy: Testing Glutaminase Inhibition for Schizophrenia Treatment in Adult Mice. *Front Syst Neurosci* **9**, 165 (2015).
34 Guardiola, O. *et al.* Cripto regulates skeletal muscle regeneration and modulates satellite cell determination by antagonizing myostatin. *Proc Natl Acad Sci U S A* **109**, E3231-3240 (2012).
35 LaFleur, M. W. *et al.* A CRISPR-Cas9 delivery system for in vivo screening of genes in the immune system. *Nat Commun* **10**, 1668 (2019).
36 Sanjana, N. E., Shalem, O. & Zhang, F. Improved vectors and genome-wide libraries for CRISPR screening. *Nat Methods* **11**, 783-784 (2014).
37 Pasut, A., Jones, A. E. & Rudnicki, M. A. Isolation and culture of individual myofibers and their satellite cells from adult skeletal muscle. *J Vis Exp*, e50074, doi:10.3791/50074 (2013).
38 Casazza, A. *et al.* Impeding macrophage entry into hypoxic tumor areas by Sema3A/Nrp1 signaling blockade inhibits angiogenesis and restores antitumor immunity. *Cancer Cell* **24**, 695-709 (2013).

ACKNOWLEDGMENTS

MM was supported by an ERC Consolidator-grant (ImmunoFit), FWO-SBO (ZL3C3602), Horizon 2020 (research and innovation program under the Marie Skłodowska-Curie grant agreement No 766214). We thank Vincent van Hoef for bioinformatic analyses; Prof. Sarah-Maria Fendt, Prof. Christian Frezza, Prof. Antonio Musarò, Prof. Giulio Cossu, Prof. Jean-Chrisophe Marine for advices; Sarah Trusso Cafarello and Sander Willox for technical support. PC and MM received long-term structural Methusalem funding by the Flemish Government; PC is supported by an ERC PoC [ERC-713758] and Advanced-grant [EU-ERC743074]. MSh is granted by China Scholarship Council (CSC); E.B. by FWO (1525315N).

AUTHOR CONTRIBUTION

MSh performed experimental design, all experiments, data acquisition and interpretation, and wrote the manuscript. FC and RA performed *in vitro* assays and histology. JS performed all the ligations and histological stainings. FV performed angiogenic and *in vitro* assays. MYR provided AAV vectors. GE performed Seahorse measurements. SC and PM generated GLUD1 cKO mice and provided critical suggestions. KDB provided the transgenic mice expressing Cre-ERT under the Pax7 promoter, and provided critical edits to the text. MSa provided critical edits to the text. PC helped in the experiments with GLS KO macrophages and provided the mice. BG and PC supported with metabolic assays and critical suggestions in manuscript writing. MDM designed and supervised all the *in vitro* and *in vivo* gene editing approaches, and provided critical edits to the text. EB performed performance experiments, histology, experimental design, data analysis, and wrote the manuscript. MM and EB performed the experimental design, data analysis, conducted scientific direction, and wrote the manuscript.

COMPETING FINANCIAL INTERESTS

No competing financial interests to declare.

DATA AVAILABILITY

RNA-seq data have been deposited to the Gene Expression Omnibus (GEO) data repository with accession number GSE123825. Source Data are provided for all the experiments. Other data that support the findings of this study are available from the corresponding author upon reasonable request.

Extended Data Table 1 | Blood count in CTRL and Glud1$^{\Delta Mo}$ mice.

The values show the haematological parameters in CTRL and Glud1$^{\Delta Mo}$ mice. Data are pooled from 2 independent experiments, CTRL *n*=8; Glud1$^{\Delta Mo}$ *n*=10. Abbreviations: white blood cell (WBC), neutrophil (NEU), lymphocyte (LYM), monocyte (MON), eosinophil (EOS), basophil (BAS), red blood cell (RBC), platelet (PLT). Values show mean ± SEM.

EXTENDED DATA FIGURE LEGENDS

Extended Data Figure 1 | Infiltrating GLUD1-deficient macrophages improve muscle repair.

a, WB for GLUD1 in BMDMs from CTRL and Glud1$^{\Delta Mo}$ mice. Vinculin was used as loading control. Representative image of 3 independent blots.

b,c, RT-qPCR of *Glud1* in F4/80^{+} macrophages (**b**), and *Glud1* in Ly6G^{+} neutrophils (**c**), sorted from TA muscles 1 day post-CTX (*n*=4).

d, Monocyte-derived macrophages (F4/80^{+} GFP^{-}) and tissue-resident macrophages (F4/80^{+} GFP^{+}) in TA muscles 1day post-CTX. Injured mice were CD68.eGFP transgenic mice reconstituted with WT (WT→CD68.eGFP) (*n*=3) or Glud1$^{\Delta Mo}$ bone marrow cells (Glud1 KO→CD68.eGFP) (*n*=4).

e, Necrotic area on H&E stained sections from TA muscles 6 days post-CTX. Injured mice were CD68.eGFP transgenic mice reconstituted with WT (WT→CD68.eGFP) or Glud1$^{\Delta Mo}$ bone marrow cells (KO→CD68.eGFP) (*n*=6). Baseline: WT→CD68.eGFP (*n*=3); KO→CD68.eGFP (*n*=4).

f, RT-qPCR of *Glud1* in F4/80^{+} macrophages, sorted from spleens upon tamoxifen-induced macrophage-specific *Glud1* deletion in Glud1$^{L/L}$;CSF1R:Cre-ERT mice (L/L in short); tamoxifen injected littermates (Glud1$^{L/L}$ and negative for CSF1R:Cre-ERT; WT in short) were used as controls (*n*=5).

g-i, Quantification of necrosis (**g**), apoptosis (**h**)**,** and regenerating fibers (**i**), from TA muscles 6 days post-CTX in tamoxifen-injected *Glud1*$^{L/L}$;CSF1R:Cre-ERT (L/L) mice and littermate controls (*Glud1*$^{L/L}$ and negative for CSF1R:Cre- ERT; WT in short) (*n*=6).

j-l, Quantification of proliferating (Ki67-expressing) SC in TA muscles (**j**) 1 day post-CTX injury (CTR *n*=4, Glud1$^{\Delta Mo}$ *n*=5), with representative images (**k**), or in crural muscles (**l**) 3 days post-ligation (*n*=5). The yellow arrows indicate Pax7^{+} Ki67^{-} cells, and the white arrows indicate Pax7^{+} Ki67^{+} cells.

m,n, WB for Pax7 in TA muscles lysates (**m**) from CTRL or Glud1$^{\Delta Mo}$ mice 1 day post-CTX (*n*=4), and densitometric quantification (**n**). Vinculin was used as loading control. Numbers represent fold change *vs.* Vinculin.

o-u, FACS quantification of total CD45^{+} leukocytes (**o**), F4/80^{+} macrophages (**p**), Ly6G^{+} neutrophils (**q**), TCRβ^{+} total T cells (**r**), CD4^{+} T cells (**s**), CD8^{+} cytotoxic T cells (**t**), and CD45R^{+} B cells (**u**), in TA muscles at baseline or 1 day post-CTX (*n*=3).

v, Laser Doppler analysis 1, 3, 6, 9 and 13 days post-ligation (CTRL *n*=5 for all the time points; Glud1$^{\Delta Mo}$ Day0/1/3/6 *n*=4, Day9/13 *n*=3). Toe perfusion of non-ligated control was defined as 100%.

w, Quantification of vessel density in crural muscles 14 days post-ligation (CTRL *n*=5; Glud1$^{\Delta Mo}$ *n*=3).

A representative (everywhere except for **n**) or a pool (**n**) of at least two independent experiments is shown. Unpaired two-tailed *t*-test was everywhere applied; ns, not significant ($P>0.05$). Scale bars: 50 μm (**k**). Graphs show mean ± SEM.

Extended Data Figure 2 |GLUD1 loss in macrophages does not alter either their recruitment or M1/M2/wound-healing gene expression patterns.

a, Crystal-violet-stained bone-marrow derived macrophages (BMDMs), migrating towards CCL21, CCL2 or PBS (Uns) in glutamine (Q)-enriched or Q-reduced media (*n*=3).

b,c, Quantification (**b**) and representative images (**c**) of F4/80 staining in ear-sections with acetone (vehicle) or upon phorbol ester (TPA)-induced cutaneous rash, 3 days and 8 days after TPA applying (Vehicle *n*=4; TPA Day3 *n*=6,5 CTRL and Glud1$^{\Delta Mo}$, respectively; TPA Day8 *n*=4).

d, Heatmap analysis of M1 and M2 macrophage gene expression in CD45^{+} F4/80^{+} macrophages sorted from TA muscles at baseline and 1 day post-CTX (*n*=4).

e, Heatmap analysis of wound healing gene expression in CD45^{+} F4/80^{+} macrophages sorted from TA muscles at baseline and 1 day post-CTX (*n*=4).

a-**c** experiments show representative values of 2 independent experiments, **d**-**e** show values from one single experiment. Unpaired two-tailed *t*-test was applied in **b**; ns, not significant (*P*>0.05). Scale bars: 50 μm (**c**). Graphs show mean ± SEM.

Extended Data Figure 3 | GLUD1 loss in macrophages does not alter either M1/M2 polarization or their related functions.

a-d, RT-qPCR of *Cxcl9* (**a**), *Tnfa* (**b**), *Arg1* (**c**), and *Il10* (**d**) in BMDMs isolated from CTRL and Glud1$^{\Delta Mo}$ mice (*n*=3).

e-h, FACS analysis of different M1 (**e, f**) or M2 (**g, h**) polarization states in CD45^{+} CD11b^{+} F4/80^{+} macrophages isolated from TA muscles at baseline (*n*=5) or 1 day post-CTX (*n*=6).

i, Quantification of macrophage phagocytosis. BMDMs were treated with LPS or PBS (unstimulated) prior to the assay (*n*=3).

j,k, Quantification (**j**), and representative images (**k**) of total endothelial sprout length of spheroid containing HUVEC and WT or Glud1$^{\Delta Mo}$ BMDMs. BMDMs were treated with IL4 prior to the assay; unstimulated BMDMs were used as control (Unstimulated *n*=7; IL4 *n*=8).

l-m, CD206^{+} F4/80^{+} area in TA muscles 1 day (n=5) and 6 days (n=8) post-CTX (**l**) or in crural muscles 3 days (CTRL *n*=6; Glud1$^{\Delta Mo}$ *n*=5), 7 days (CTRL *n*=7; Glud1$^{\Delta Mo}$ *n*=5) and 14 days (CTRL *n*=6; Glud1$^{\Delta Mo}$ *n*=5) post-ligation (**m**).

All experiments show representative values of at least 2 independent experiments. Unpaired two-tailed *t*-test was everywhere applied**;** ns, not significant (*P*>0.05). Scale bars: 50 µm (**k**). Graphs show mean ± SEM.

Extended Data Figure 4 | GLUD1 loss in macrophages enhances GS-mediated glutamine release.

a, Quantification (by GC-MS) of intracellular 2-oxoglutarate content in BMDMs cultured in Q-enriched or Q-reduced media (*n*=3).

b,c, LC-MS measurement of total cellular energy charge ([ATP + 1/2ADP]/[ATP + ADP + AMP]) (**b**) and ATP content (**c**) in BMDMs (*n*=3).

d, Oxygen consumption rate (OCR) in BMDMs (*n*=5).

e-f, Quantification of intracellular (**e**) and extracellular (**f**) glutamine content in BMDMs cultured in Q-enriched or Q-reduced media (*n*=3).

g, [U-^{14}C]-glutamine uptake in BMDMs cultured in Q-enriched (*n*=4) or Q-reduced (WT *n*=4; Glud1$^{\Delta Mo}$ *n*=3) media.

h, Evaluation of [U-^{13}C]-glutamine-derived carbon incorporation into glutamate in BMDMs (*n*=3).

i-j, Evaluation of [U-^{13}C]-glucose-derived carbon incorporation levels into 2-oxoglutarate (**i**) and glutamate (**j**) in BMDMs (*n*=3).

k-l, Quantification of intracellular (**k**) and extracellular (**l**) glutamine content in BMDMs upon silencing of BCAT1 or BCAT2 (*n*=3).

m-n, Quantification of intracellular (**m**) and extracellular (**n**) glutamine content in BMDMs upon silencing of GOT1 or GOT2 (*n*=3).

o, Quantification of SC on TA muscles 1 day post-CTX injury, stained for PHH3 and Pax7. CTRL and Glud1$^{\Delta Mo}$ mice were treated 2 times per day with the BCAT1 inhibitor Gabapentin, or vehicle as control (*n*=6).

p, Fold change in glutamate to leucine ratio in the interstitial fluid of TA muscles 1day post-CTX, relative to PBS-injected CTRL muscle (PBS *n*=6; CTX *n*=9).

q, Fold change in glutamate to leucine ratio in the interstitial fluid of crural muscles 3 days post-ligation, relative to CTRL baseline muscle (Baseline *n*=7,8 CTRL, Glud1$^{\Delta Mo}$, respectively; ligated *n*=11,12 CTRL, Glud1$^{\Delta Mo}$, respectively).

r, Evaluation of the conversion of glutamate to 2-OG by analyzing [U-^{13}C]-glutamine (Q-enriched condition) or [U-^{13}C]-glutamate (Q-reduced condition) incorporation into 2-OG in WT BMDMs (*n*=3).

s, Evaluation of the conversion of 2-OG to glutamate by analyzing $^{15}NH_4^+$ incorporation into glutamate in WT BMDMs (*n*=3).

t, Evaluation of glutamine synthetase (GS) activity by analyzing $^{15}NH_4^+$ incorporation into glutamine in BMDMs (*n*=3).

u,v, Evaluation of the conversion of GLUD1 activity (**u**)**,** and glutamine synthetase (GS) activity (**v**)**,** in muscle-infiltrating macrophages, sorted 1 day post-CTX. One unit for the conversion of glutamate to 2-OG is the amount of enzyme that will generate 1 µmole of NADH per minute at pH 7.6 at 37°C. One unit of GS activity is defined as the enzyme producing 1 nmole of gamma-glutamyl hydroxamic acid per minute (CTRL *n*=4; Glud1$^{\Delta Mo}$ *n*=3). The control condition (CTRL) in **u**,**v** is the same one displayed in Fig. 2p at day 1.

All experiments (except for **o**) show representative values of at least 2 independent experiments, **o** shows values from one single experiment. Unpaired two-tailed *t*-test was everywhere applied; ns, not significant ($P>0.05$); a.u., arbitrary unit. Graphs show mean ± SEM.

Extended Data Figure 5 | Harnessing glutamine uptake *in vitro*.

a,b, Quantifications (**a**) and representative images (**b**) of myotube diameter in C2C12 cells cultured in BMDM-conditioned media (CM) (*n*=3 except for Q-reduced C2C12 where *n*=2).

c, RT-qPCR of SLC1A5 knockdown efficiency in C2C12 cells. Cells were transduced with a LV co-expressing Cas9 and a gRNA targeting the *Slc1a5* locus (SLC1A5-KD) (*n*=5) or a non-targeting control gRNA (Ctrl gRNA) (*n*=4).

d, [U-^{14}C]-glutamine uptake in SLC1A5-deficient C2C12 cells (SLC1A5 KD) generated by co-expressing Cas9 along with a gRNA targeting the *Slc1a5* locus. Parental cells (CTRL) and cells transduced with a non-targeting control gRNA (Ctrl gRNA) were used as negative controls. C2C12 cells treated with SLC1A5 inhibitor gamma-L-Glutamyl-p-Nitroanilide (GPNA) were used as a positive control (*n*=3).

e-f, Quantification (**e**) and representative images (**f**) of myotube diameter in control or SLC1A5-KD C2C12 cells co-cultured with BMDMs under glutamine deprivation (*n*=3 except Ctrl C2C12 *n*=2).

g, RT-qPCR analysis of the proliferation marker *Pcna* in control or SLC1A5-KD C2C12 cells, or control C2C12 treated with the mTOR inhibitor Torin2, cultured for 18 hours in BMDM-conditioned, Q-reduced growth media, where the only glutamine present comes from WT or GLUD1 KO BMDMs. A non-targeting control gRNA (Ctrl gRNA) was used as control (*n*=3).

h, RT-qPCR analysis of the differentiation marker *Myogenin* in control or SLC1A5-KD C2C12 cells, or control C2C12 treated with the mTOR inhibitor Torin2, cultured for 72 hours in BMDM-conditioned, Q-reduced differentiation media, where the only glutamine present comes from WT or GLUD1 KO BMDMs. A non-targeting control gRNA (Ctrl gRNA) was used as control (*n*=3).

i, Representative images of an immunofluorescence for Pax7 on a pure SC population, freshly isolated from hindlimb muscles of WT mice.

j, RT-qPCR for *Slc1a5* in SC, transduced with the same LV as above. The graph shows values of 3 biological repetitions per condition.

k-l, Quantification (**k**) and representative images (**l**) of EdU by immunofluorescence in control or SLC1A5-KD SC. A non-targeting control gRNA (Ctrl gRNA) was used as a control (Ctrl gRNA *n*=5; SLC1A5-KD *n*=6).

m-o, Quantification (**m,n**) and representative images (**o**) of fusion index and myotube size in control or SLC1A5-KD SC 5 days of culture in differentiation media. A non-targeting control gRNA (Ctrl gRNA) was used as a control. The graph shows values of 3 biological repetitions per condition.

All experiments show representative values of at least 2 independent experiments. Unpaired two-tailed *t*-test was everywhere applied; ns, not significant ($P>0.05$). Scale bars: 50 µm (**b,f,l**); 100 µm (**o**). Graphs show mean ± SEM.

Extended Data Figure 6 | Selective and inducible knockdown of *Slc1a5* in SC.

a, Schematic representation of the AAV8 expression vector for *in vivo* targeting of SC. U6, Pol III promoter driving the expression of the gRNA targeting the *Slc1a5* locus or a non-targeting control gRNA. Since the mice used in this experiment are LSL-Cas9 x PAX7:Cre-ERT mice, Cas9 is exclusively activated in $Pax7^{+}$ cells upon tamoxifen administration and, genome editing of the *Slc1a5* locus will occur selectively in SC.

b, Schematic overview of an AAV8-based CRISPR/Cas9-mediated *in vivo* genome editing.

c-d, Representative images (**c**) and quantification (**d**) for Pax7 and Cas9 staining on uninjured muscles before and after tamoxifen administration (*n*=4).

e-f, RT-qPCR for *Slc1a5* in freshly isolated SC (n=4) (**e**) and all other mononuclear cells (non-SC) (*n*=3) (**f**) upon *in vivo* genome editing of the *Slc1a5* locus (SLC1A5-KD) specific in SC. Non-targeting control gRNA (Ctrl gRNA) was used as a control.

g-h, Quantification (**g**) and representative images (**h**) of SLC1A5 and Pax7 stainings on freshly isolated SC, upon *in vivo* genome editing of the *Slc1a5* locus (SLC1A5-KD) specific in SC (*n*=3).

All experiments show representative values of at least 2 independent experiments. Unpaired two-tailed *t*-test was everywhere applied; ns, not significant ($P>0.05$). Scale bars: 50 µm (**c**); 20 µm (**h**). Graphs show mean ± SEM.

Extended Data Figure 7 | *Slc1a5* knockdown in SC impairs the recovery of the muscle from CTX-induced damage.

a-d, Quantification of TUNEL$^+$ cells (**a**), F4/80$^+$ area (**c**) and representative images (**b**,**d**) respectively, in TA muscle 6 days post-CTX obtained from LSL-Cas9 x PAX7:Cre-ERT mice treated with an AAV8 vector encoding for Ctrl gRNA (Ctrl gRNA) or *Slc1a5* gRNA (SLC1A5-KD) (*n*=4).

e,f, Quantification (**e**) and representative images (**f**) of EdU$^+$ myonuclei in TA muscle 6 days post-CTX, upon *in vivo* genome editing of the *Slc1a5* locus (SLC1A5-KD) specific in SC. EdU was given by i.p. injection at 24h, 48h and 72h after CTX injection (*n*=6).

a-d show representative values of 2 independent experiments, **e-f** show values of 1 experiment. Unpaired two-tailed *t*-test was everywhere applied; ns, not significant (*P*>0.05). Scale bars: 20 µm (**b,d,f**). Graphs show mean ± SEM.

Extended Data Figure 8 | Macrophage-specific genetic deletion or pharmacologic inhibition of GLUD1 alters only the basal inflammation and weight of muscle tissue in aged mice.

a, Representative images of $F4/80^+$ area in crural muscles of young and aged mice.

b-i, Quantification and representative images of $F4/80^+$ area in brain (**b,c**), liver (**d,e**), lung (**f,g**), and skin (**h,i**) of aged mice (n=5 except in **b** for $Glud1^{\Delta Mo}$ *n*=4).

j-n, Body weight (**j**) and mass to body weight ratio of kidney (**k**), liver (**l**), spleen (**m**), and fat tissues (**n**) of aged mice upon R162 treatment (CTRL *n*=5; $Glud1^{\Delta Mo}$ *n*=6).

a-**i** show representative values of at least 2 independent experiments, **j**-**n** show values of 1 experiment. Unpaired two-tailed *t*-test was everywhere applied, ns, not significant (*P*>0.05). Scale bars: 50 µm (**a,i**); 20 µm (**c,e,g**). Graphs show mean ± SEM.

Extended Data Figure 9 | GLS loss in macrophages is not advantageous for muscle repair.

a,b, [U-^{14}C]-glutamine uptake (**a**) and glutamine oxidation (**b**) in WT or GLS KO BMDMs cultured with Q-enriched or Q-reduced media (*n*=3).

c,d, 2-oxoglutarate (2-OG) to succinate ratio in WT or GLS KO BMDMs (**c**) and 2-OG to succinate ratio in WT or GLUD1 KO BMDMs (**d**). BMDMs were treated with 50ng/mL LPS or PBS (unstimulated) prior to the assay (*n*=3).

e, Evaluation of GS activity by analyzing the percentage of the $^{15}NH_4^+$-derived ammonia incorporation levels into glutamine in BMDMs isolated from CTRL and Gls $^{\Delta Mo}$ mice (*n*=3).

f, Fold change in glutamine to glutamate ratio in the interstitial fluid of TA muscle 1 day post-CTX, relative to PBS injected CTRL muscle (*n*= 6).

g,h, Quantification of necrotic (right side of the graph) and regenerating (left side of the graph) areas on H&E-stained sections from TA muscles 6 days post-CTX (n= 6) (**g**) and representative images (**h**).

i,j, Quantification (**i**) and representative images (**j**) of TUNEL$^+$ cells in TA muscle 6 days post-CTX (*n*=6).

k-m, Representative images (**k**) and quantification of F4/80$^+$ area (**l**), CD206$^-$ F4/80$^+$ cells (M1) to CD206$^+$ F4/80$^+$ cells (M2) ratio (**m**) in TA muscles 6 days post-CTX (*n*=6).

n-q, RT-qPCR of *Tnfa* (**n**), *Cxcl9* (**o**), *Mrc1* (**p**) and *Retnla* (**q**) in BMDMs isolated from CTRL and Gls$^{\Delta Mo}$ mice. BMDMs were treated with LPS or PBS (unstimulated) prior to the assay (*n*=3).

r, Scheme illustrating the physiological role of Glud1 in macrophages in response to muscle damage. During muscle disruption, ischemia or aging, interstitial glutamine drops likely because of the loss in myofibers (a major glutamine source) and poor blood supply. Infiltrating macrophages respond to glutamine starvation by reducing their oxidative GLUD1 activity in favour of GS activity. Macrophage-derived glutamine is released and progressively fills the muscle interstitium, where it is uptaken by SC promoting their proliferation and differentiation into new fibers, two processes that are favoured by glutamine-dependent mTOR activation. Towards the end of this regenerative process, the newly generated fibers will undertake glutamine production while inflammation will be progressively resolved. GLUD1-deficient macrophages are metabolically pre-adapted towards glutamine synthesis and release, thus preventing this glutamine drop. It follows that, in case of muscle damage, macrophage-specific knockout of Glud1 or pharmacologic GLUD1 blockade strengthens SC activation, ultimately leading to therapeutic muscle regeneration.

All experiments show representative values of at least 2 independent experiments. Unpaired two-tailed *t*-test was everywhere applied; ns, not significant (*P*>0.05). Scale bars: 20 μm (**h**); 10 μm (**j,k**). Graphs show mean ± SEM.

1253

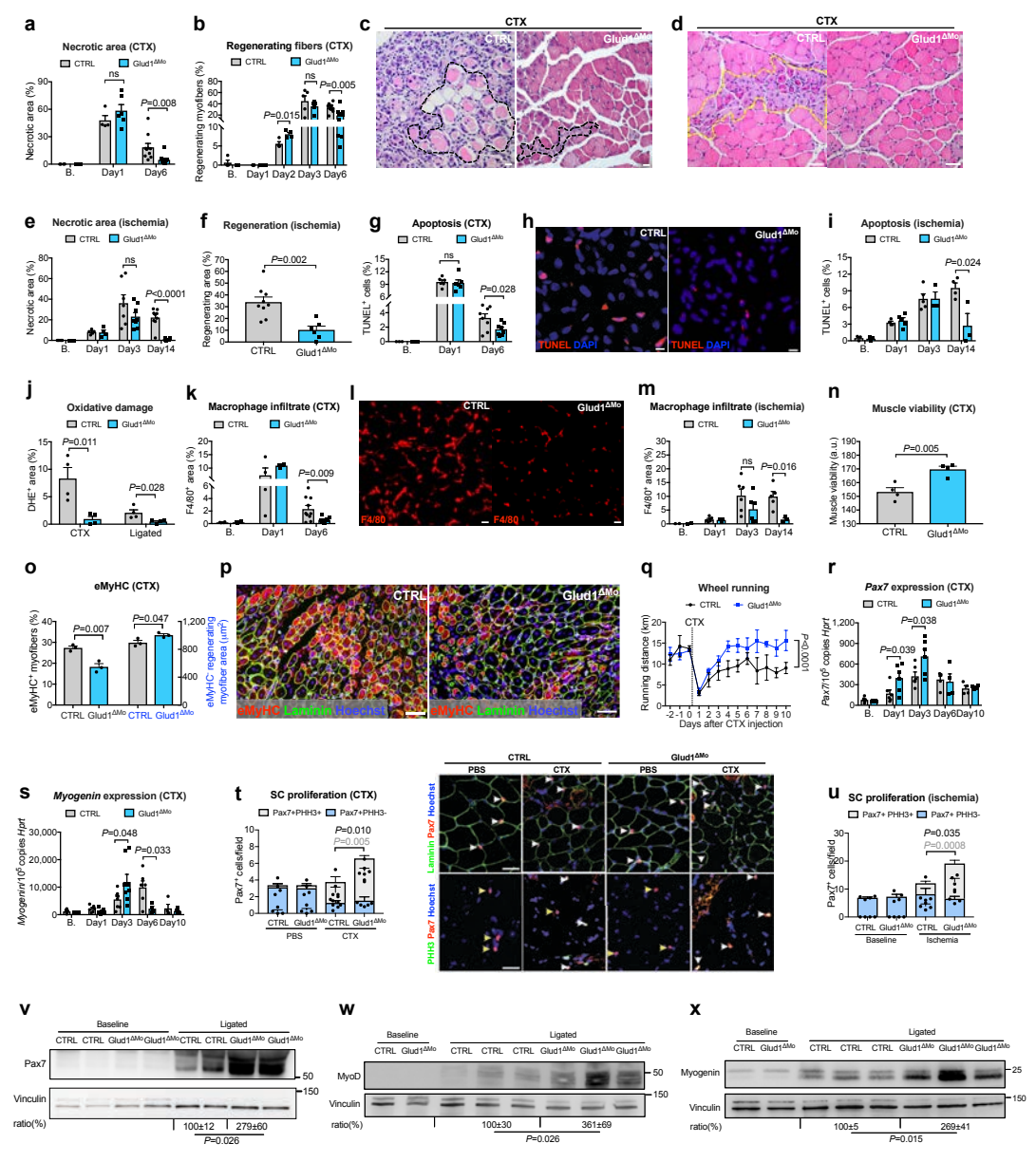
a
Necrotic area (CTX)
CTRL
Glud1ΔMo
Necrotic area (%)
ns
P=0.008
B.
Day1
Day6
b
Regenerating fibers (CTX)
Regenerating myofibers (%)
P=0.015
ns
P=0.005
B.
Day1
Day2
Day3
Day6
c
CTX
CTRL
Glud1ΔMo
d
CTX
CTRL
Glud1ΔMo
e
Necrotic area (ischemia)
Necrotic area (%)
ns
P<0.0001
B.
Day1
Day3
Day14
f
Regeneration (ischemia)
Regenerating area (%)
P=0.002
CTRL
Glud1ΔMo
g
Apoptosis (CTX)
TUNEL+ cells (%)
ns
P=0.028
B.
Day1
Day6
h
CTRL
Glud1ΔMo
TUNEL DAPI
TUNEL DAPI
i
Apoptosis (ischemia)
TUNEL+ cells (%)
P=0.024
B.
Day1
Day3
Day14
j
Oxidative damage
DHE+ area (%)
P=0.011
P=0.028
CTX
Ligated
k
Macrophage infiltrate (CTX)
F4/80+ area (%)
P=0.009
B.
Day1
Day6
l
CTRL
Glud1ΔMo
F4/80
F4/80
m
Macrophage infiltrate (ischemia)
F4/80+ area (%)
ns
P=0.016
B.
Day1
Day3
Day14
n
Muscle viability (CTX)
Muscle viability (a.u.)
P=0.005
CTRL
Glud1ΔMo
o
eMyHC (CTX)
eMyHC+ myofibers (%)
P=0.007
P=0.047
eMyHC+ regenerating myofiber area (µm²)
CTRL
Glud1ΔMo
CTRL
Glud1ΔMo
p
CTRL
Glud1ΔMo
eMyHC Laminin Hoechst
eMyHC Laminin Hoechst
q
Wheel running
CTRL
Glud1ΔMo
CTX
Running distance (km)
P<0.0001
Days after CTX injection
r
Pax7 expression (CTX)
CTRL
Glud1ΔMo
Pax7/10⁶ copies Hprt
P=0.038
P=0.039
B.
Day1
Day3
Day6
Day10
s
Myogenin expression (CTX)
CTRL
Glud1ΔMo
Myogenin/10⁶ copies Hprt
P=0.048
P=0.033
B.
Day1
Day3
Day6
Day10
t
SC proliferation (CTX)
Pax7+PHH3+
Pax7+PHH3-
Pax7+ cells/field
P=0.010
P=0.005
CTRL
Glud1ΔMo
CTRL
Glud1ΔMo
PBS
CTX
CTRL
Glud1ΔMo
PBS
CTX
Laminin Pax7 Hoechst
PHH3 Pax7 Hoechst
u
SC proliferation (ischemia)
Pax7+ PHH3+
Pax7+ PHH3-
Pax7+ cells/field
P=0.035
P=0.0008
CTRL
Glud1ΔMo
CTRL
Glud1ΔMo
Baseline
Ischemia
v
Baseline
Ligated
CTRL CTRL Glud1ΔMo Glud1ΔMo CTRL CTRL Glud1ΔMo Glud1ΔMo
Pax7
Vinculin
50
150
ratio(%)
100±12
279±60
P=0.026
w
Baseline
Ligated
CTRL Glud1ΔMo
CTRL CTRL CTRL Glud1ΔMo Glud1ΔMo Glud1ΔMo
MyoD
Vinculin
50
150
ratio(%)
100±30
361±69
P=0.026
x
Baseline
Ligated
CTRL Glud1ΔMo
CTRL CTRL CTRL Glud1ΔMo Glud1ΔMo Glud1ΔMo
Myogenin
Vinculin
25
150
ratio(%)
100±5
269±41
P=0.015

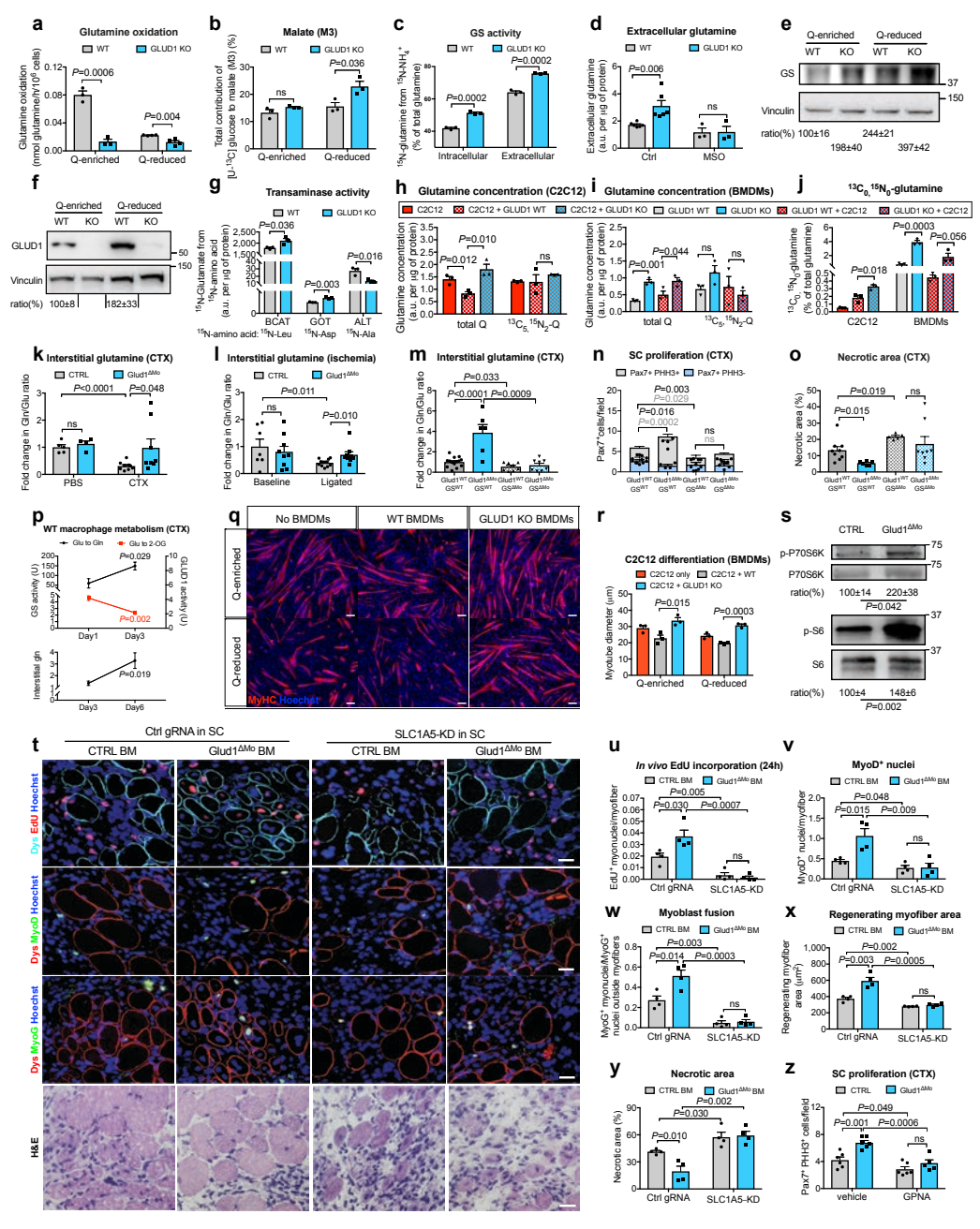
a
Glutamine oxidation
WT
GLUD1 KO
Glutamine oxidation (nmol glutamine/hr/10⁶ cells)
P=0.0006
P=0.004
Q-enriched
Q-reduced
b
Malate (M3)
Total contribution of [U-13C] glucose to malate (M3) (%)
ns
P=0.036
c
GS activity
15N-glutamine from 15NH4+ (% of total glutamine)
P=0.0002
P=0.0002
Intracellular
Extracellular
d
Extracellular glutamine
Extracellular glutamine (a.u. per ug of protein)
P=0.006
ns
Ctrl
MSO
e
Q-enriched
Q-reduced
WT
KO
GS
Vinculin
37
150
ratio(%) 100±16 244±21 198±40 397±42
f
GLUD1
Vinculin
50
150
ratio(%) 100±8 182±33
g
Transaminase activity
15N-Glutamate from 15N-amino acid (a.u. per ug of protein)
P=0.036
P=0.003
P=0.016
BCAT
GOT
ALT
15N-amino acid: 15N-Leu 15N-Asp 15N-Ala
h
Glutamine concentration (C2C12)
C2C12
C2C12 + GLUD1 WT
C2C12 + GLUD1 KO
Glutamine concentration (a.u. per ug of protein)
P=0.010
P=0.012
ns
total Q
13C5, 15N2-Q
i
Glutamine concentration (BMDMs)
GLUD1 WT
GLUD1 KO
GLUD1 WT + C2C12
GLUD1 KO + C2C12
Glutamine concentration (a.u. per ug of protein)
P=0.044
P=0.001
ns
ns
total Q
13C5, 15N2-Q
j
13C5, 15N2-glutamine
15N2-glutamine (% of total glutamine)
P=0.0003
P=0.056
P=0.018
C2C12
BMDMs
k
Interstitial glutamine (CTX)
CTRL
Glud1ΔMo
Fold change in Gln/Glu ratio
P<0.0001
P=0.048
ns
PBS
CTX
l
Interstitial glutamine (ischemia)
CTRL
Glud1ΔMo
Fold change in Gln/Glu ratio
P=0.011
ns
P=0.010
Baseline
Ligated
m
Interstitial glutamine (CTX)
Fold change in Gln/Glu ratio
P=0.033
P<0.0001
P=0.0009
Glud1WT GS WT
Glud1ΔMo GS WT
Glud1WT GS ΔMo
Glud1ΔMo GS ΔMo
n
SC proliferation (CTX)
Pax7+ PHH3+
Pax7+ PHH3-
Pax7+cells/field
P=0.003
P=0.029
P=0.016
P=0.0002
ns
ns
o
Necrotic area (CTX)
Necrotic area (%)
P=0.019
ns
P=0.015
p
WT macrophage metabolism (CTX)
Glu to Gln
Glu to 2-OG
GS activity (U)
Glu to 2-OG activity (U)
P=0.029
P=0.002
Day1
Day3
Interstitial gln
P=0.019
Day3
Day6
q
No BMDMs
WT BMDMs
GLUD1 KO BMDMs
Q-enriched
Q-reduced
MyHC Hoechst
r
C2C12 differentiation (BMDMs)
C2C12 only
C2C12 + WT
C2C12 + GLUD1 KO
Myotube diameter (μm)
P=0.015
P=0.0003
Q-enriched
Q-reduced
s
CTRL
Glud1ΔMo
p-P70S6K
P70S6K
75
75
ratio(%) 100±14 220±38
P=0.042
p-S6
S6
37
37
ratio(%) 100±4 148±6
P=0.002
t
Ctrl gRNA in SC
SLC1A5-KD in SC
CTRL BM
Glud1ΔMo BM
Dys EdU Hoechst
Dys MyoD Hoechst
Dys MyoG Hoechst
H&E
u
In vivo EdU incorporation (24h)
CTRL BM
Glud1ΔMo BM
EdU+ myonuclei/myofiber
P=0.005
P=0.030
P=0.0007
ns
Ctrl gRNA
SLC1A5-KD
v
MyoD+ nuclei
MyoD+ nuclei/myofiber
P=0.048
P=0.015
P=0.009
ns
Ctrl gRNA
SLC1A5-KD
w
Myoblast fusion
MyoG+ myonuclei/MyoG+ nuclei of each myofibers
P=0.003
P=0.014
P=0.0003
ns
Ctrl gRNA
SLC1A5-KD
x
Regenerating myofiber area
Regenerating myofiber area (μm²)
P=0.002
P=0.003
P=0.0005
ns
Ctrl gRNA
SLC1A5-KD
y
Necrotic area
Necrotic area (%)
P=0.002
P=0.030
P=0.010
Ctrl gRNA
SLC1A5-KD
z
SC proliferation (CTX)
CTRL
Glud1ΔMo
Pax7+ PHH3+ cells/field
P=0.049
P=0.001
P=0.0006
ns
vehicle
GPNA

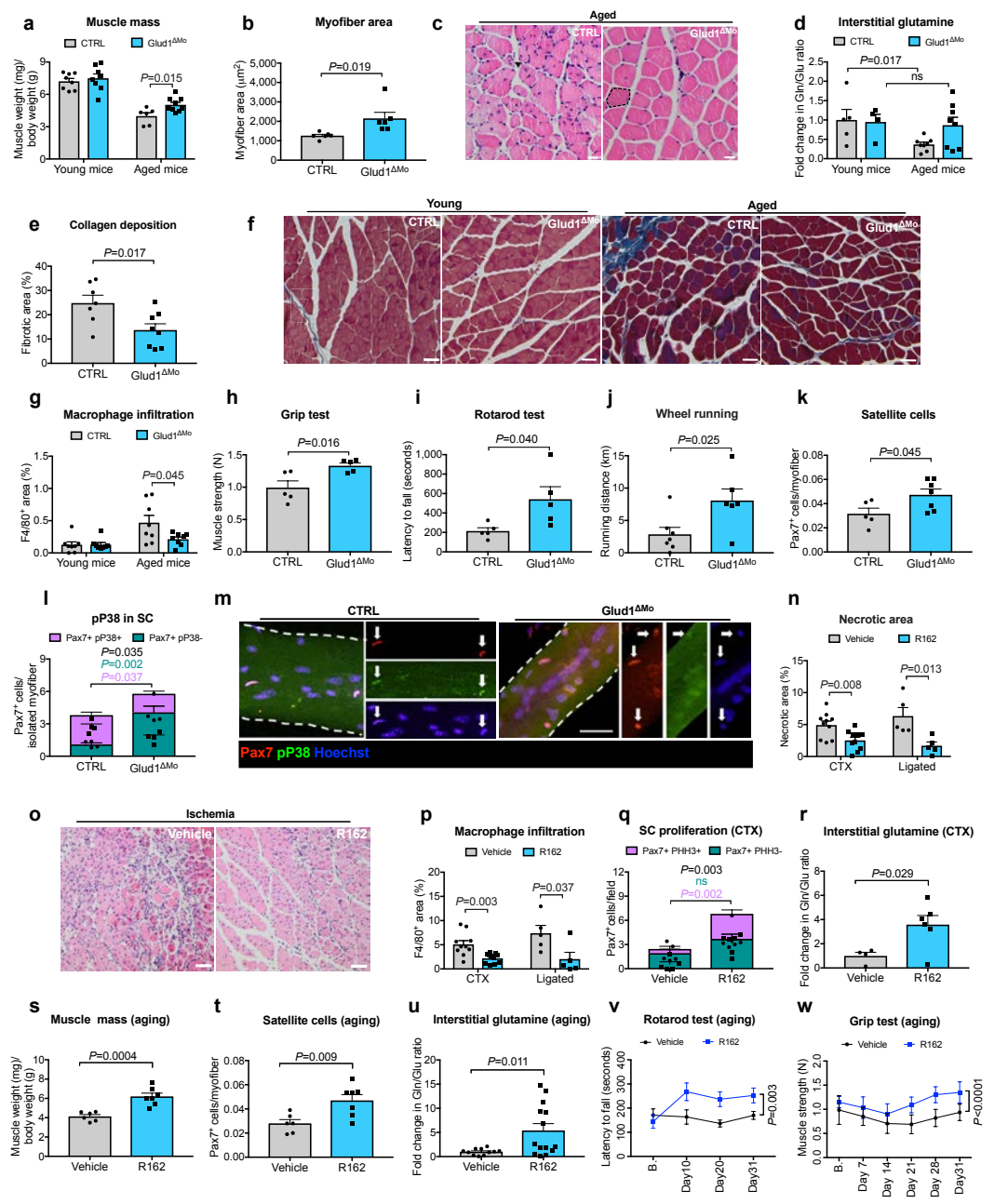
a
Muscle mass
CTRL
Glud1ΔMo
Muscle weight (mg)/ body weight (g)
P=0.015
Young mice
Aged mice
b
Myofiber area
Myofiber area (µm2)
P=0.019
CTRL
Glud1ΔMo
c
Aged
CTRL
Glud1ΔMo
d
Interstitial glutamine
CTRL
Glud1ΔMo
Fold change in Gln/Glu ratio
P=0.017
ns
Young mice
Aged mice
e
Collagen deposition
Fibrotic area (%)
P=0.017
CTRL
Glud1ΔMo
f
Young
Aged
CTRL
Glud1ΔMo
CTRL
Glud1ΔMo
g
Macrophage infiltration
CTRL
Glud1ΔMo
F4/80+ area (%)
P=0.045
Young mice
Aged mice
h
Grip test
Muscle strength (N)
P=0.016
CTRL
Glud1ΔMo
i
Rotarod test
Latency to fall (seconds)
P=0.040
CTRL
Glud1ΔMo
j
Wheel running
Running distance (km)
P=0.025
CTRL
Glud1ΔMo
k
Satellite cells
Pax7+ cells/myofiber
P=0.045
CTRL
Glud1ΔMo
l
pP38 in SC
Pax7+ pP38+
Pax7+ pP38-
P=0.035
P=0.002
P=0.037
Pax7+ cells/ isolated myofiber
CTRL
Glud1ΔMo
m
CTRL
Glud1ΔMo
Pax7 pP38 Hoechst
n
Necrotic area
Vehicle
R162
Necrotic area (%)
P=0.008
P=0.013
CTX
Ligated
o
Ischemia
Vehicle
R162
p
Macrophage infiltration
Vehicle
R162
F4/80+ area (%)
P=0.003
P=0.037
CTX
Ligated
q
SC proliferation (CTX)
Pax7+ PHH3+
Pax7+ PHH3-
Pax7+cells/field
P=0.003
ns
P=0.002
Vehicle
R162
r
Interstitial glutamine (CTX)
Fold change in Gln/Glu ratio
P=0.029
Vehicle
R162
s
Muscle mass (aging)
Muscle weight (mg)/ body weight (g)
P=0.0004
Vehicle
R162
t
Satellite cells (aging)
Pax7+ cells/myofiber
P=0.009
Vehicle
R162
u
Interstitial glutamine (aging)
Fold change in Gln/Glu ratio
P=0.011
Vehicle
R162
v
Rotarod test (aging)
Vehicle
R162
Latency to fall (seconds)
P=0.003
B.
Day10
Day20
Day31
w
Grip test (aging)
Vehicle
R162
Muscle strength (N)
P<0.0001
B.
Day 7
Day 14
Day 21
Day 28
Day31